UNITED NATIONS UNIVERSITY
GEOTHERMAL TRAINING PROGRAMME
Orkustofnun, Grensásvegur 9,
IS-108 Reykjavík, Iceland

Reports 2007
Number 11

MAGNETOTELLURIC AND TRANSIENT ELECTROMAGNETIC METHODS IN GEOTHERMAL EXPLORATION, WITH AN EXAMPLE FROM TENDAHO GEOTHERMAL FIELD, ETHIOPIA

Yohannes Lemma
Geological Survey of Ethiopia
Hydrogeology, Engineering Geology and Geothermal Department
P.O. Box 2302, Addis Ababa
ETHIOPIA
yohlema@yahoo.com

ABSTRACT

Electromagnetic methods (EM) are frequently used in the exploration of geothermal resources for determining the spatial distribution of electrical resistivity (conductivity). Magnetotellurics (MT) and time domain electromagnetic (TEM) methods are especially used for geothermal exploration when using EM methods. Geothermal resources are ideal targets for EM methods since they produce strong variations in underground electrical resistivity (conductivity). Electrical resistivity is directly related to parameters that characterize geothermal systems. In this report, the application of TEM and MT methods and interpretation of data from the Tendaho geothermal field in Ethiopia are discussed.

TEM data were used to correct for static shift in MT data from the same site. MT data were analyzed and modelled using 1D Occam inversion of the determinant of the impedance tensor. A low resistivity at shallow depth is interpreted as a sedimentary formation, lateral flow of geothermal fluids or a fracture zone. The high resistivity below the low resistivity can be associated with less permeable Afar stratoid series basalts. An observed low-resistivity zone bounded between high-resistivity zones is interpreted as a fracture zone in the Afar stratoid basalts which may give rise to higher permeability and higher temperature and may indicate upflow of geothermal fluid. The fracture zones inferred from MT correlate with NW-SE trending structures from gravity and magnetic surveys and the surface geothermal manifestations in the area. The fracture zones are not well resolved because of large MT station spacing. Therefore, it is recommended that additional TEM (with large loop area) and systematically gridded long period MT surveys should be carried out to delineate the size and boundary of the geothermal resource in the Tendaho geothermal field.

1. INTRODUCTION

Geophysical methods play a key role in geothermal exploration since many objectives of geothermal exploration can be achieved by using them. A geothermal system generally causes inhomogeneities in the physical properties of the subsurface, which can be observed to varying degrees as anomalies

measurable from the surface (Manzella, 2007). The geophysical surveys are directed at obtaining indirectly, from the surface or from shallow depth, the physical parameters of the geothermal system. These physical parameters include temperature, electrical conductivity, and elastic properties influencing the propagating velocity of elastic waves, density and magnetic susceptibility. Electrical methods have proven to be a powerful tool in geothermal exploration for decades. Their preference is a result of the direct relationship of resistivity to parameters that characterize geothermal systems (Hersir and Björnsson, 1991). These important parameters are porosity, permeability, temperature, chemical composition of the fluid and hydrothermal alteration.

Electrical geophysical prospecting methods detect the surface effects produced by electric currents flowing in the ground. Using electrical methods, one may measure potentials, currents, and electromagnetic fields which occur naturally or those introduced artificially in the ground. Geothermal resources are ideal targets for electromagnetic (EM) methods since they produce strong variations in underground electrical resistivity. In thermal areas, the electrical resistivity is substantially different and generally lower than in areas with colder subsurface temperature (Oskooi et al., 2004).

In this report, geophysical methods applied in geothermal exploration, especially electromagnetic methods, will be discussed. A survey from the Tendaho geothermal field in Ethiopia is used as an example of the application of these methods.

2. GEOPHYSICAL METHODS IN GEOTHERMAL EXPLORATION

Various parameters are measured in geophysical exploration. Geophysical methods are divided into direct and indirect or structural methods (Hersir and Björnsson, 1991). Direct methods include the thermal method and the electrical method. Gravity, magnetic, and seismic methods are indirect methods.

The most direct method for studying geothermal systems is that of *subsurface temperature measurements (thermal method)*. Measurements can be made in holes as shallow as a few metres or in soil, but the preference at the present time is to conduct temperature surveys in wells that are at least 100 m deep (Manzella, 2007). Thermal surveys can delineate areas of enhanced thermal gradient, which is a basic requirement for a high-enthalpy geothermal system, and define the temperature distribution.

Gravity surveys are used for geothermal exploration to define density variation related to deep magmatic bodies, which may represent a heat source. Gravity monitoring surveys are also performed in geothermal areas to monitor the change in groundwater level and together with subsidence monitoring.

The magnetic method is useful in mapping near-surface features such as faults and dikes that are often of interest in geothermal exploration, but the greatest potential for the method lies in its ability to detect the depth at which the Curie temperature is reached. Ferromagnetic materials exhibit a phenomenon characterised by a loss of nearly all magnetic susceptibility at a critical temperature called the Curie temperature (Manzella, 2007).

Seismic methods can be divided into two main subclasses: passive seismic methods and active seismic methods. Passive seismic methods deal with natural earthquakes or those induced by fracturing related to geothermal fluid extraction and injection. Active seismic methods cover all seismic prospecting having an artificial wave source. Many geothermal systems occur mainly in areas characterised by a relatively high level of micro seismic activity. However, there does not appear to be a one-to-one relationship between the locations of micro earthquakes and the presence of

geothermal reservoirs. Passive seismic methods detect seismic activity and can give information about sound velocity, attenuation and S-wave shadows. Seismic activity gives information about active faults and permeable zones (Hersir and Björnsson, 1991).

Geophysical well logs are performed to give information on well performance, and also to obtain information on the lithological structure and physical properties of the geothermal system penetrated by the well.

Several variations of *direct current resistivity methods* have been used for decades in geothermal exploration with success (Hersir and Björnsson, 1991). The most widely used is the Schlumberger method. DC-methods are used both for depth sounding and profiling.

Electromagnetic soundings are made to determine variations in the electrical conductivity of the earth with depth. Electromagnetic (EM) sounding methods include natural-field methods (magneto telluric and audiomagnetotellurics), and controlled-source induction methods, as well as high-frequency radiation techniques such as radar-probing. Because of the depth of the main targets in geothermal exploration, only natural-source and controlled-source methods (time domain electromagnetic) are used (Manzella, 2007).

3. RESISTIVITY METHODS IN GEOTHERMAL EXPLORATION

Measuring the electrical resistivity of the subsurface is the most powerful prospecting method in geothermal exploration (Hersir and Björnsson, 1991). Resistivity is directly related to the properties of interest, such as, temperature, alteration, salinity and porosity/permeability (Hersir and Björnsson, 1991).

3.1 Resistivity of rocks

The resistivity of a material is defined as the resistance in ohms between the opposite faces of a unit cube of the material (Kearey and Brooks, 1994). For a conducting cylinder of resistance (R), length (L) and cross-sectional area (A) the resistivity is given by:

$$\rho = \frac{RA}{L} \tag{1}$$

where ρ = Resistivity of the material (Ωm);
R = Resistance (Ω);
L = Length (m);
A = Area of the conducting cross-section (m^2).

The electric current in a short, thin, linear conductor of uniform cross-section is given by Ohm's law as:

$$I = -\frac{dV}{R} \tag{2}$$

where I = Electric current (A);
dV = Potential difference (V) between the ends of a conductor with a length *dl.*

From Equations 1 and 2 we get:

$$\frac{I}{A} = -\frac{1}{\rho}\frac{dV}{dl}$$

This (Ohm's law) can be written as:

$$j = \frac{E}{\rho} \qquad \text{or} \qquad j = \sigma E \tag{3}$$

where j = I/A= Current density (Am^{-2});
E = $-dV/dl$ = Electric field ($V\ m^{-1}$);
σ = Conductivity of the material ($S\ m^{-1}$)

The conductivity (σ) of a material is defined as the reciprocal of its resistivity (ρ).

Most rock forming minerals and rock matrices are electrical insulators. Measured resistivity in earth materials is primarily controlled by the movement of charged ions in pore fluids and rock-water interface. The electrical resistivity of rocks depends mainly on the following parameters (Hersir and Björnsson, 1991):

a) Porosity and permeability of the rock;
b) Salinity of the water;
c) Temperature; and
d) Water-rock interaction and alteration

a) Porosity / Permeability
Porosity is the ratio between pore volume and the total volume of a material. This is given by the ratio as:

$$\phi = \frac{V_V}{V_T} \tag{4}$$

where ϕ = Porosity;
V_v = Volume of void space (m^3);
V_T = Total or bulk volume of the material (m^3).

The resistivity of water-saturated rocks often varies approximately as the inverse power of the porosity according to an empirical formula given by Archie (1942):

$$\rho = \rho_w\ a\ {\phi_t}^{-n} \tag{5}$$

where ρ = Bulk (measured) resistivity (Ωm);
ρ_w = Resistivity of the pore fluid (Ωm);
ϕ = Porosity
a and n = Empirical constants.

Archie´s law can also be written as:

$$\rho = F\ \rho_w \tag{6}$$

where F = $a\ {\phi_t}^{-n}$ = Formation factor.

In some rocks, part of the pore space may be occupied by air (above the water table) or by natural gas, carbon dioxide or petroleum, all of which are insulators. In such cases, Archie's law is modified as follows (Zhdanov and Keller, 1994):

$$\rho = \rho_w a\ {\phi_t}^{-n}\ f^{-c} \tag{7}$$

where f = Fraction of pores containing water of resistivity ρ_w
c = Empirical constant

Experiments show that Archie's law is only valid for conductive solutions, with $\rho_w \leq 2$ Ωm (Flóvenz et al., 1985).

Permeability is the capacity of a porous material for transmitting a fluid; it is expressed as the amount of fluid of specified viscosity, under the influence of a given pressure that passes through a sample having a certain cross-section and thickness. Permeability is largely dependent on the size and shape of the pores in the substance and, in granular materials such as sedimentary rocks, by the size, shape, and packing arrangement of the grains. The permeability of a rock is given by the following equation:

$$K = \frac{Q\eta L}{AP} \tag{8}$$

where K = Permeability (m^2);
Q = Fluid flowrate (m^3/s);
η = Fluid viscosity (kg/ms);
L = Length of the rock (m);
A = Cross-sectional area available for flow (m^2); and
P = Pressure drop (Pa).

b) Salinity
An increase in the total amount of dissolved ions can increase the conductivity by large amounts (Figure 1). The conductivity of a solution depends on mobility and concentration of the ions. This is given by the equation (Hersir and Björnsson, 1991):

$$\sigma = \frac{1}{\rho} = F(c_1 q_1 m_1 + c_2 q_2 m_2 + \cdots) \tag{9}$$

where σ = Conductivity (S/m);
F = Faraday´s number (96500 coulombs);
c_i = Concentration of ions;
q_i = Valence of ions;
m_i = Mobility of different ions.

An increase in the water content and an increase in the total amount of dissolved solids are associated with geothermal activity.

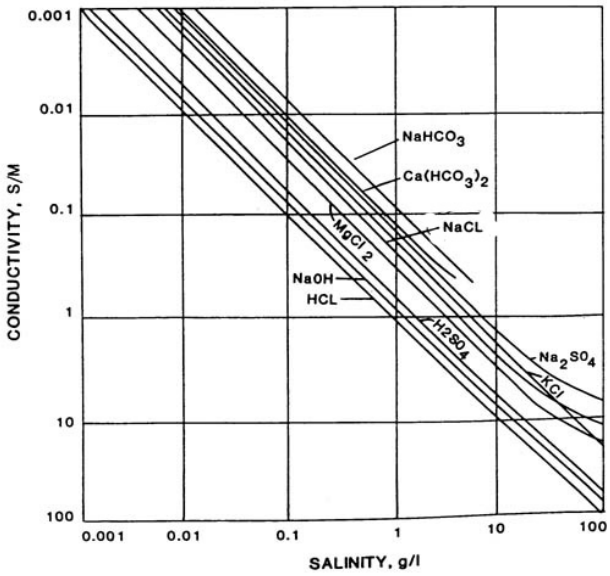

FIGURE 1: Conductivity vs. salinity for different Electrolytes (Keller and Frischkecht, 1966)

c) Temperature
At moderate temperatures, 0-200°C, resistivity of aqueous solutions decreases with increasing temperature (Figure 2). This is due to an increase in ion mobility caused by a decrease in the viscosity of the water. Dakhnov (1962) has described this relationship:

$$\rho_w = \frac{\rho_{wo}}{1+\alpha(T-T_o)} \tag{10}$$

where ρ_w = Resistivity of the fluid at temperature T (Ωm);
ρ_{wo} = Resistivity of the fluid at temperature T_o (Ωm);
α = Temperature coefficient of resistivity ($°C^{-1}$).

At high temperatures, a decrease in the dielectric permittivity of the water results in a decrease in the number of dissociated ions in solution. Above 300°C, fluid resistivity starts to increase (Quist and Marshall, 1968).

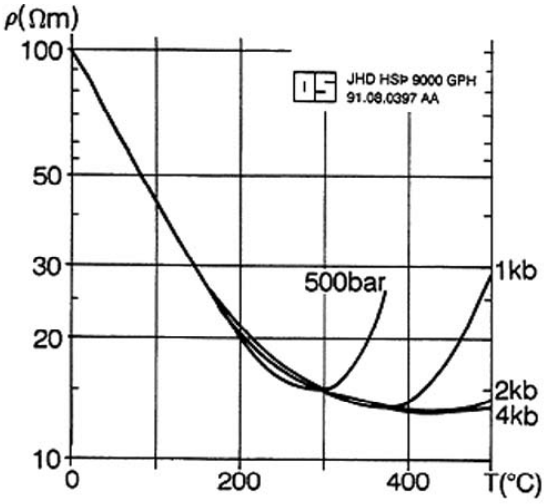

FIGURE 2: Electrical resistivity as a function of temperature at different pressures (from Quist and Marshall, 1968)

d) Water-rock interaction and interface conduction
Apart from the reduction in resistivity by the pore fluid, the bulk resistivity of the rock is also reduced by the presence of hydrous secondary minerals (such as clays) as a result of fluid-rock interaction. This interface conductivity (alteration) is expressed by the equation (Hersir and Björnsson, 1991):

$$\sigma = \frac{1}{F}\,\sigma_w + \sigma_s \qquad (11)$$

where σ = Bulk conductivity (S/m);
σ_w = Conductivity of water (S/m);
σ_s = Interface conductivity (S/m);
F = Formation factor of the rock.

The interface conductivity, σ_s, is caused by fluid-matrix interaction and depends mostly on the magnitude of the internal surfaces (porosity) and of their nature (surface conditions). The main two reasons for surface conductivity are the presence of clay minerals (alteration) and surface double-layer conduction.

The alteration process and the resulting type of alteration minerals are dependent on the type of primary minerals, and the chemical composition of the geothermal fluid and temperature. The intensity of the alteration is furthermore dependent on the temperature, time and texture of the host rocks. Alteration intensity is normally low for temperatures below 50°C. At temperatures lower than 220°C, low-temperature zeolites and the clay mineral smectite are formed. Smectite has hydrated and loosely bound cations between the silica plates, making the mineral conductive and with a high cation exchange capacity (Árnason et al., 2000).

In the temperature range from 220 to about 240-250°C, the low-temperature zeolites disappear and the smectite is transformed into chlorite in a transition zone, the so-called mixed-layered clay zone, where smectite and chlorite coexist in a mixture. At about 250°C the smectite disappears and chlorite is the dominant mineral, marking the beginning of the chlorite zone, hence, with increased resistivity, since chlorite minerals have cations that are fixed in a crystal lattice, making the mineral resistive. At still higher temperatures, about 260-270°C, epidote becomes abundant in the so-called chlorite-epidote zone (Árnason et al., 2000).

3.2 Electrical methods overview

Electrical methods employ a variety of measurements of the effects of electrical current flow within the earth. The phenomena that can be measured include current flow, electrical potential (voltage), and electromagnetic fields (Colorado School of Mines, 1999). Electrical methods can be divided into the following categories and subcategories (Hersir and Björnsson, 1991):

a) DC methods
This is an active method that employs measurement of electrical potential associated with subsurface electrical current flow generated by a DC, or slowly varying AC source. Two main types of measurements can be distinguished, and a third mentioned:

- *Resistivity sounding*. Measurements are made at a specified fixed centre point for different distances between the electrodes. It is used to measure variations in resistivity with depth.

Example: In Schlumberger sounding the potential electrodes remain fixed and the current electrodes are expanded along a line symmetrically about the centre of the profile.

- *Resistivity profiling*. Electrode arrangement with fixed distances is used and measurements are made as all the array is moved along a profile. It is designed to locate lateral variation in resistivity. Example: Head-on profiling.
- *Self potential (SP)*. This is a passive method that employs measurements of naturally occurring electrical potentials.

b) Electromagnetic (EM) methods

- *Magnetotellurics (MT) and audio-magnetotellurics (AMT)*. The fluctuations in the natural magnetic field of the earth and the induced electric field are measured. Their ratio is used to determine the apparent resistivity.
- *Time domain or transient electromagnetic (TEM)*. A magnetic field is built up by transmitting a constant current into a loop or grounded dipole, the current is turned off and the transient decay of the magnetic field is measured.

The central-loop TEM sounding method has several advantages over conventional DC sounding methods (Árnason, 1989). The transmitter couples inductively to the earth and no current has to be injected into the ground. This is of great importance in areas where the surface is highly resistive (Árnason, 1989). Secondly, the fact that the monitored signal is a decaying magnetic field, rather than an electric field at the surface, makes the results much less dependant on local resistivity conditions at the receiver site (Sternberg et al., 1988). Distortions due to local resistivity inhomogeneities at the receiver site can be a severe problem in DC sounding as well as in MT soundings (Árnason, 1984). Thirdly, the central-loop TEM is less sensitive to lateral resistivity variations than the DC methods. TEM soundings are much more downward-focused than DC soundings. One-dimensional inversion is better justified in the interpretation of central-loop TEM soundings than in DC soundings. In Schlumberger soundings, the monitored signal is low when surveying over low-resistivity structures like a geothermal area, whereas in TEM soundings it is relatively strong (Árnason, 1989).

Electromagnetic techniques have proven to be among the most useful geophysical methods for the investigation of geothermal regions. This is due to the fact that the spatial distribution of conductivity in a geothermal area is not only determined by the host rock distribution, but is directly related to the distribution of the actual exploration target - hot water (Berktold, 1983).

3.3 TEM method

In the central-loop TEM sounding method, a loop of wire is placed on the ground and a constant magnetic field of known strength is built up by transmitting a constant current into the loop (Figure 3). The current is then abruptly turned off. The decaying magnetic field induces electrical current in the ground. The current distribution in the ground induces a secondary magnetic field decaying with time (Figure 4). The decaying rate of the secondary magnetic field is monitored by measuring the voltage induced in the receiver coil at the centre of the transmitter loop. The current distribution and the decay rate of the secondary magnetic field depend on the resistivity structure of the earth. The

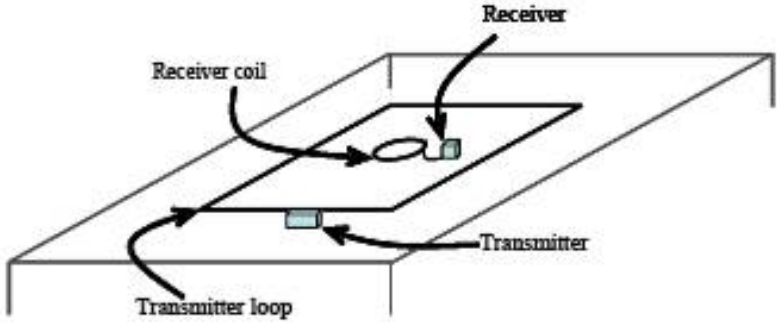

FIGURE 3: Central-loop TEM configuration

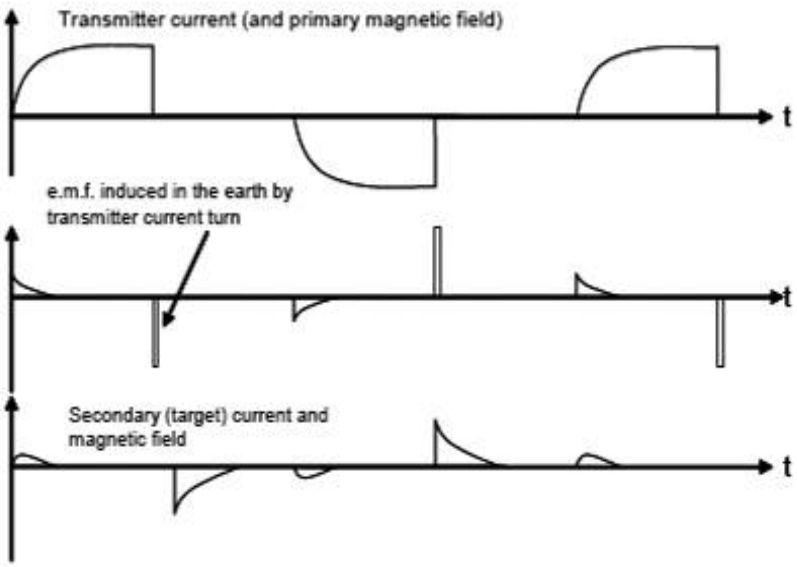

FIGURE 4: Transmitted and received waveforms in a typical time-domain system (Ward and Wannamaker, 1983)

decay rate, recorded as a function of time after the current in the transmitter loop is turned off can, therefore, be interpreted in terms of a subsurface resistivity structure (Árnason, 1989).

In a central-loop TEM configuration, the induced voltage in a receiver coil (in the frequency domain) on top of N-layered earth, due to alternating current transmitted into a loop, is given by (Árnason 1989):

$$V_c(\omega, r) = A_r n_r A_s n_s I_o e^{i\omega t} \frac{-i\omega\mu_0}{\pi r} \int_0^\infty \frac{\lambda^2}{m_0} \frac{S_0}{S_0 - T_0} J_1(\lambda r) d\lambda \tag{12}$$

where A_r = Cross-sectional area of the receiver coil (m^2)
n_r = Number of windings in the coil
μ_o = Magnetic permeability in vacuum (H/m)
A_s = Cross-sectional area of transmitter loop (m^2)
n_s = Number of windings in the loop
$J_1(\lambda r)$ = Bessel function of first order

S_o and T_o are given by the recursion relations:

$$S_{i-1} = S_i \cosh(m_i d_i) - T_i \sinh(m_i d_i) \tag{13}$$

$$T_{i-1} = -\frac{m_i}{m_{i-1}} [S_i \sinh(m_i d_i) - T_i \cosh(m_i d_i)] \tag{14}$$

$$S_{N-1} = 1; \qquad T_{N-1} = -\frac{m_N}{m_{N-1}} \tag{15}$$

where d_i = Thickness of the i^{th} layer;
m_i = Electrical parameter of i^{th} layer = $\sqrt{\lambda^2 - k_i^2}$;
k_i^2 $\approx -i\omega\mu_i\sigma_i$ (quasi-stationary approximation); and
ω = Angular frequency.

The mutual impedance (Z_c) between the source and the receiver in a central-loop configuration is defined as the ratio between the measured voltage and the transmitted current is given by:

$$Z_c(\omega, r) = \frac{V_c(\omega, r)}{I_0 e^{i\omega t}} = A_r n_r A_s n_s \frac{-i\omega\mu_0}{\pi r} \int_0^\infty \frac{\lambda^2}{m_0} \frac{S_0}{S_0 - T_0} J_1(\lambda r) d\lambda \tag{16}$$

The transmitter step current function *I(t)* can be written as:

$$I(t) = \frac{1}{(2\pi)^{1/2}} \int_{-\infty}^{\infty} \tilde{I}(\omega) e^{i\omega t}\, d\omega \tag{17}$$

where

$$\check{I}(\omega) \quad = \frac{1}{(2\pi)^{1/2}} \int_{-\infty}^{\infty} I(t) e^{-i\omega t}\, dt = \frac{I_o}{-i\omega}$$

The induced voltage as a function of time in the receiver in terms of mutual impedance as a function of frequency and the Fourier transform of the transmitted current follows from Equation 16 and is given as:

$$V_c(t,r) = \frac{1}{(2\pi)^{1/2}} \int_{-\infty}^{\infty} Z_c(\omega, r)\, \tilde{I}(\omega) e^{i\omega t}\, d\omega \tag{18}$$

The measured voltage as a function of time after a steady current (square wave form) is abruptly turned off at time t=0 is given by:

$$V(t) = \frac{-\mathrm{I}_0}{2\pi} \int_{-\infty}^{\infty} \frac{Z(\omega)}{i\omega} e^{-i\omega t}\, d\omega = \frac{I_0}{2\pi} \int_{-\infty}^{\infty} \phi(\omega)\, e^{-i\omega t} d\omega \tag{19}$$

where

$$\phi(\omega) = \frac{Z(\omega)}{-i\omega} \tag{20}$$

From Equations 14 and 20 it can be seen that $\phi(\omega)$ only depends on ω through ω^2 and $i\omega$. This implies that:

$$\phi^*(-\omega) = \phi(\omega) \tag{21}$$

where * denotes the complex conjugate, and thus:

$$Re\ \phi(-\omega) = Re\ \phi(\omega); \quad Im\ \phi(-\omega) = -Im\ \phi(\omega) \tag{22}$$

Therefore, Equation 19 can be rewritten as:

$$V(t) = \frac{2I_0}{\pi} \int_0^{\infty} Re\ \phi(\omega) \cos(\omega t)\, d\omega \tag{23}$$

The measured voltage due to a ramped step function with ramp length, or turn-off time *TOFF* according to Árnason (1989) is given by:

$$\mathrm{V(t)} = \frac{I_0}{TOFF} \int_{-TOFF}^{0} v(t-\tau) d\tau = \frac{I_0}{TOFF} \int_{t}^{t+TOFF} v(\tau) d\tau \tag{24}$$

where $v(t)$ = Unit step response.

In the case of homogenous earth of conductivity σ, and late times after the current in the transmitter is abruptly turned off, the transient voltage is approximately given by (Árnason, 1989):

$$V_c(r,t) \approx \frac{C_c\, (\mu_0\, \sigma r^2)^{3/2}}{10\pi^{1/2}\, t^{5/2}} \tag{25}$$

where $C_c = A_r n_r A_s n_s \frac{\mu_0}{2\pi r^3}$

This shows that the transient voltage is proportional to $\sigma^{3/2}$ and falls off with time as $t^{-5/2}$.

From Equation 25 with $\rho = 1/\sigma$, the late time apparent resistivity of the central-loop TEM configuration is given by:

$$\rho_a(r,t) = \frac{\mu_0}{4\pi}\left(\frac{2\mu_0 A_r n_r A_s n_s I_0}{5t^{5/2}V\,(r,t)}\right)^{2/3} \tag{26}$$

where t = Time elapsed after the current in the transmitter loop is turned off (s);
A_r = Cross-sectional area of the receiver coil (m^2);
n_r = Number of windings in the coil;
μ_o = Magnetic permeability in vacuum (H/m);
A_s = cross-sectional area of loop (m^2);
n_s = Number of windings in the loop;
I_o = Transmitter current (A);
$V(r, t)$ = Measured voltage (V).

The transient response for a homogenous half space can be plotted as a logarithm of output voltage versus a logarithm of time (Figure 5). The response can be divided into an early stage, intermediate stage and late stage. During the late stage, the measured voltage is decaying at a rate of $t^{-5/2}$, which is very rapid with time. Eventually the signal disappears into noise, and further measurement is impossible. This defines the maximum depth of exploration for a particular system (McNeill, 1994).

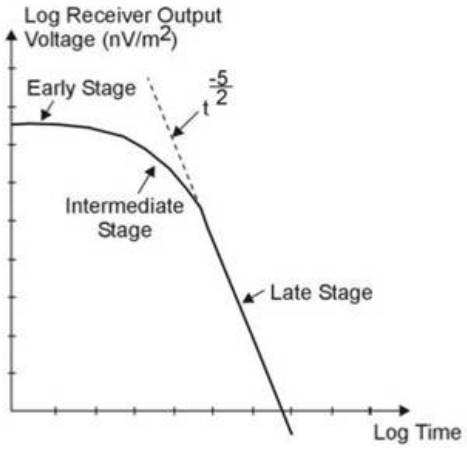

FIGURE 5: Receiver output voltage vs. time

At early and intermediate times, Figure 5 shows that the receiver voltage is below the extrapolated $t^{-5/2}$ line and, thus, from Equation 26, the apparent resistivity will be too high. For this reason, there will always be, as shown in Figure 6, a "descending branch" at early time where the apparent resistivity is higher than the half-space resistivity (ρ_1). But at late time, the apparent resistivity $\rho_a\ (t)$ is equal to ρ_1 which is the true resistivity of the layer (McNeill, 1994).

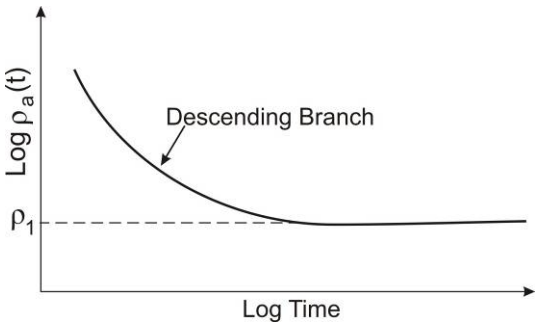

FIGURE 6: Apparent resistivity for homogeneous half space

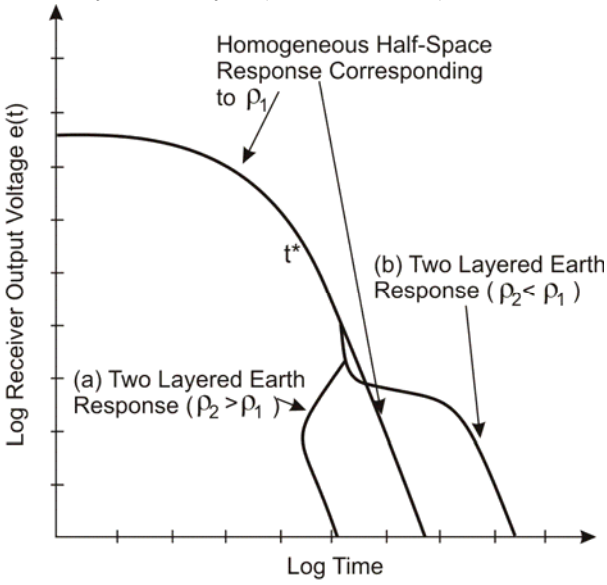

FIGURE 7: Receiver output voltage for two-layered earth

For a two-layered earth of upper layer resistivity ρ_1 , and thickness h, and basement resistivity ρ_2 , at early time when the currents are entirely in the upper layer of resistivity ρ_1 , the decay curve will look like that of Figure 5, and the apparent resistivity curve will look like Figure 6 (McNeill, 1994). However, later on the currents will lie in both layers, and at much later time, they will be located entirely in the basement, of resistivity ρ_2. If $\rho_2>\rho_1$, Equation 26 shows that the measured voltage will be less than it should have been for the homogeneous half-space of resistivity ρ_1 (Figure 7a). The effect on the apparent resistivity curve is shown in Figure 8a. Since at late times all the currents are in the

basement, the apparent resistivity $\rho_a(t)$ becomes equal to ρ_2. If $\rho_2 < \rho_1$, the inverse behaviour is also as expected, i.e., at late times the measured voltage response, Figure 7b, is greater than that from a homogeneous half-space of resistivity ρ_1, and the apparent resistivity curve correspondingly becomes that of Figure 8b, becoming equal to the new value of ρ_2 at late time. For the case of a conductive basement ($\rho_2 < \rho_1$), there is a region of intermediate time t^* (Figure 7), where the voltage response temporarily falls (undershoot) before continuing on to adopt the value appropriate to ρ_2. The resultant influence of the anomalous behaviour on the apparent resistivity is also shown as overshoot in Figure 8b at t^* (McNeill, 1994).

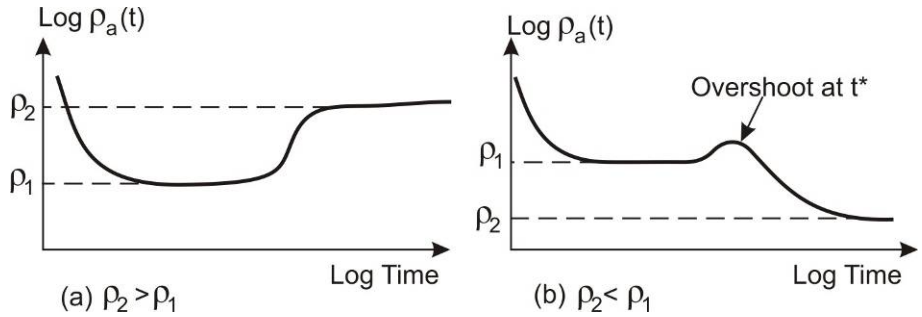

FIGURE 8: Apparent resistivity curves for two layered earth

3.4 MT method

The magnetotelluric (MT) method is a passive electromagnetic technique that involves measuring fluctuations in the natural electric field, *E*, and magnetic field, *H*, in orthogonal directions at the surface of the Earth as a means of determining the conductivity structure of the earth at depths ranging from a few tens of meters to several hundreds of kilometres (Simpson and Bahr, 2005) (Figure 9).

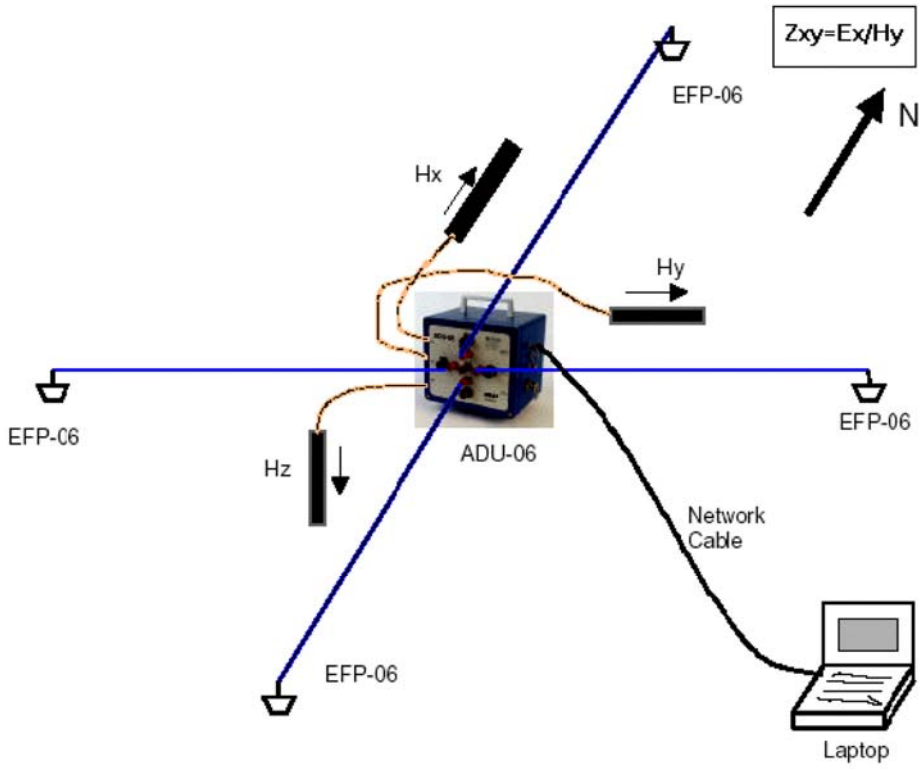

FIGURE 9: A typical 5-channel MT field setup (taken from ADU-06's Manual)

The magnetic field fluctuations are produced mainly by the interaction between the solar wind and the ionosphere. In addition, worldwide thunderstorm activity causes magnetic fields at frequencies above 1 Hz. These natural phenomena create strong MT source signals over the entire frequency spectrum. The variations are measured over a wide range of frequencies (1/10,000 to 10,000 Hz).

The depth to which EM waves penetrate into a uniform ground of resistivity ρ before becoming attenuated is characterized by the skin depth (δ). Skin depth is defined as the depth where the electromagnetic field has reduced to e^{-1} of its original value at the surface:

$$\delta = \left(\frac{2}{\omega\mu\sigma}\right)^{1/2} \tag{27}$$

Therefore, the capacity of the electromagnetic field to yield information about conductivity at depth increases as the frequency decreases or the period of oscillation increases.

Magnetic induction source field **H** penetrates vertically into geological formations and induces an electric field vector **E** in the subsurface material. The source field is related to the induced field through a transfer relationship involving an impedance tensor **Z** given by (Dobrin, 1988):

$$\mathbf{E} = \mathbf{ZH} \tag{28}$$

where **E**, **H** and **Z** are functions of frequency.

In a Cartesian coordinate system (x, y) Equation 28 can be expressed by the matrix equation:

$$\begin{pmatrix} \mathrm{E_x} \\ \mathrm{E_y} \end{pmatrix} = \begin{pmatrix} \mathrm{Z_{xx}} & \mathrm{Z_{xy}} \\ \mathrm{Z_{yx}} & \mathrm{Z_{yy}} \end{pmatrix} \begin{pmatrix} \mathrm{H_x} \\ \mathrm{H_y} \end{pmatrix} \tag{29}$$

The wave impedance or Cagniard impedance Z of homogenous ground is given by (Zhdanov and Keller, 1994):

$$\mathbf{Z} = \begin{pmatrix} 0 & \mathrm{Z} \\ -\mathrm{Z} & 0 \end{pmatrix}; \qquad Z = \frac{E_x}{H_y} = -\frac{E_y}{H_x} = \frac{i\omega\mu}{k} \tag{30}$$

where Z = Impedance of a medium (V/A or Ω);
ω = Angular frequency (Hz);
μ = Magnetic permeability (H/m);
σ = Conductivity of medium (S/m);
E_x = Electric field strength (V/m) in x direction;
H_y = Magnetic Field strength (T or Tesla) in y direction;
k = $\sqrt{i\omega\mu(\sigma + i\omega\varepsilon)}$ = wave propagation number;
ε = Dielectric permittivity (C/ V m).

At low frequencies $k^2 = i\omega\mu\sigma$, and Z further reduces to:

$$Z = \sqrt{\mu\omega\rho}.e^{i\pi/4} \tag{31}$$

Z is complex, being composed of both real and imaginary parts. In Equation 31, $\pi/4 = 45°$ is the phase difference between E_x and H_y with E_x leading H_y (Figure 10). For non-homogenous earth, the apparent resistivity, ρ_a (Ωm) is defined by:

$$\rho_a = \frac{1}{\mu\omega}|Z|^2 \tag{32}$$

Similarly, the phase of the complex impedance function is defined by:

$$\phi = \tan^{-1}\left(\frac{Im\, Z}{Re\, Z}\right) \tag{33}$$

For a 1-D Earth, where conductivity varies only with depth, the diagonal elements of the impedance tensor, Z_{xx} and Z_{yy} are zero, whilst the off-diagonal components are equal in magnitude, but have opposite signs, i.e., $Z_{xy} = -Z_{yx}$. For a 2-D Earth, in which conductivity varies along one horizontal direction as well as depth, Z_{xx} and Z_{yy} are equal in magnitude, but have opposite signs, whilst Z_{xy} and Z_{yx} differ. For a 2-D Earth with the x- or y-direction aligned along electromagnetic strike, Z_{xx} and Z_{yy} are again zero. In the general 3D case, all four components of the impedance tensor and their corresponding apparent resistivities are non-zero.

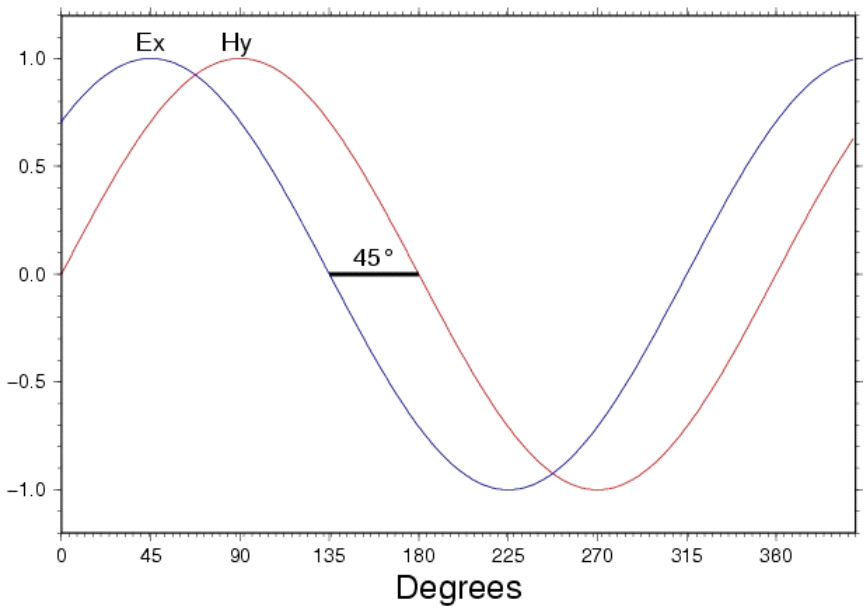

FIGURE 10: Homogeneous half-space response of electric and magnetic field intensity

For 2D earth after rotation to a principle (strike) direction, two apparent resistivities based on off-diagonal impedances are given by:

$$\rho_{xy} = \frac{1}{\omega\mu}\left|Z_{xy}\right|^2 \text{ and } \rho_{yx} = \frac{1}{\omega\mu}\left|Z_{yx}\right|^2 \tag{34}$$

The effective impedance tensor Z_{eff} is rotationally invariant and is given by the determinant of the impedance matrix in Equation 29:

$$Z_{eff} = \left(Z_{xx}Z_{yy} - Z_{xy}Z_{yx}\right)^{1/2} \tag{35}$$

Consequently:

$$\rho_{eff} = \frac{1}{\omega\mu}\left|Z_{eff}\right|^2 \quad \text{and} \quad \phi_{eff} = \text{phase of } \left|Z_{xx}Z_{yy} - Z_{xy}Z_{yx}\right| \tag{36}$$

For horizontally *N*-layered earth, the plane wave impedance is given by the recursion formula (Ward and Wannamaker, 1983):

$$\hat{Z}_{n-1} = Z_{n-1}\,\frac{\hat{Z}_n + Z_{n-1}\tanh(ik_{n-1}h_{n-1})}{Z_{n-1} + \hat{Z}_n\tanh(ik_{n-1}h_{n-1})} \quad \text{for n= N-1,...1} \tag{37}$$

where Z_n = $i\mu\omega/k_n$ (intrinsic impedance of the n^{th} layer); with
k_n = $\sqrt{(i\omega\mu\sigma_n)}$;
h_n = Thickness of the n^{th} layer;
$\hat{Z}_1$ = $\hat{Z}_0$ = Impedance on the surface.

Surficial bodies can severely distort magnetotelluric (MT) apparent resistivity data to arbitrarily low frequencies. This distortion, known as the MT static shift, is due to an electric field generated from boundary charges on surficial inhomogeneities, and persists throughout the entire MT recording range. Static shifts are manifested in the data as vertical, parallel shifts of log-log apparent resistivity sounding curves, the impedance phase being unaffected (Pellerin and Hohmann, 1990).

Electromagnetic methods which only measure magnetic fields such as TEM do not have the static shift problems that afflict MT sounding (Simpson and Bahr, 2005). Therefore, TEM data can be used in conjunction with MT data from the same site in order to correct for static shifts (Sternberg et al., 1988).

4. TEM AND MT SURVEY AT TENDAHO GEOTHERMAL FIELD

4.1 Location and geography of the study area

The Tendaho geothermal field is located in the central part of the Afar Depression, about 600 km from Addis Ababa in the northeast part of Ethiopia (Figure 11). Structurally the area is part of the Tendaho graben, which is about 50 km wide, 100 km long and oriented in a NW-SE direction. The study area is confined within the flat zones of Tendaho geothermal field (Tendaho plantation) with an average elevation of 365 m. Some peaks exist with altitudes ranging from 400 to 625 m, the highest being the Kurub volcano (Figure 11).

The Afar region, as a whole, has an arid climate with occasional rain from June to September. The Awash river flows throughout the year in the Tendaho area and is used for irrigation. The region is inhabited by Afar people, whose livelihood is dependent on small scale farming and cattle breeding.

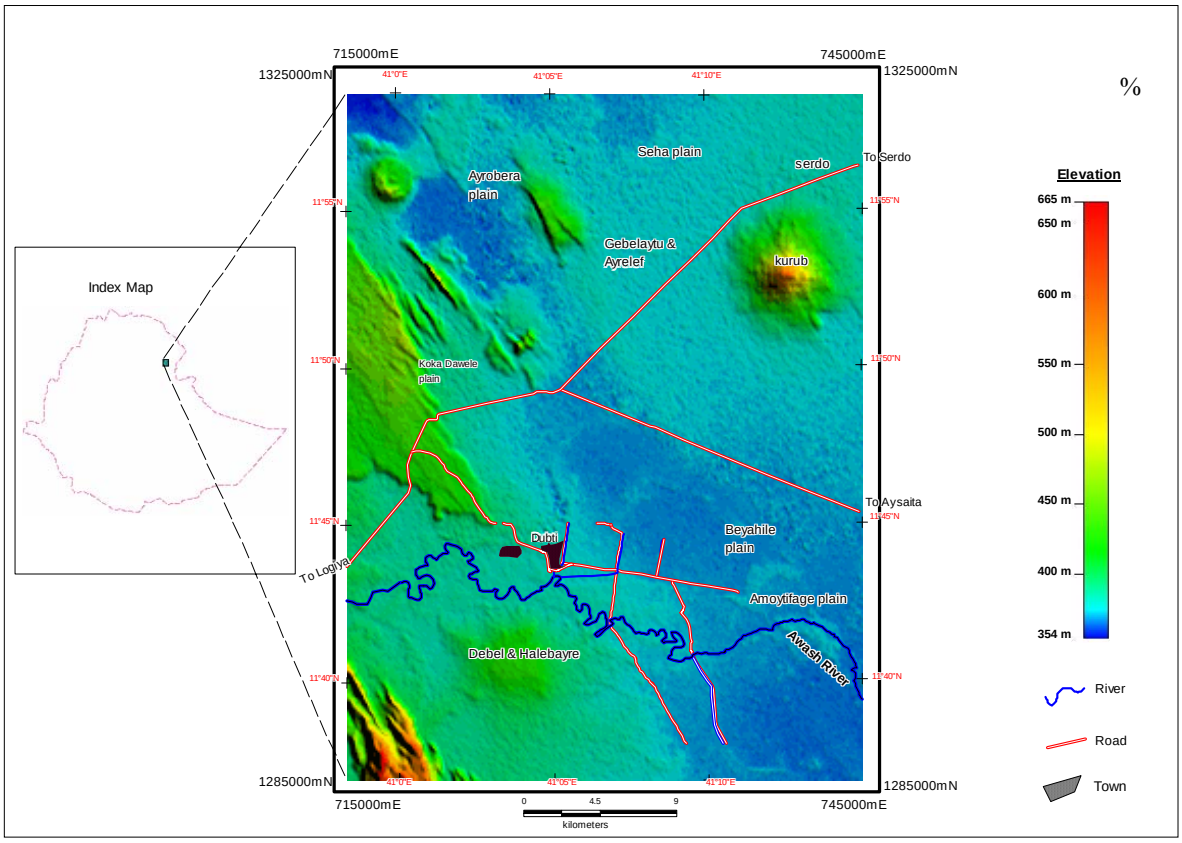

FIGURE 11: Location map of the study area

Currently, settlement in townships at the Semera, Logya, and Dubti localities is increasing. The Tendaho graben is transversed by an excellent highway that serves as the main transport route for Ethiopia's foreign trade through Djibouti. Accessibility to the project area is very good.

4.2 Review of previous work

4.2.1 Geologic and tectonic setting

Tendaho graben trends in a northwesterly direction in the southern portion of the Erta-Manda Hararo rift system in the Afar region (Aquater, 1995). The rift joins the Ethiopian rift close to the Dama Ale volcano, west of Lake Abhe. The Tendaho rift, however, does not merely swerve into the main Ethiopian rift, but is prolonged east of the latter by the Gobaad structure (Aquater, 1996). The borders of the Tendaho rift are constituted by the Afar Stratoid series and the rift is filled with lacustrine and alluvial deposits and with post stratoid basalt flows. This filling is topped by recent volcanoes, including the historically active Kurub and Damal Ale volcanoes (Aquater, 1996). The Tendaho graben is bounded by the Logya fault to the west and the Gamare fault to the east. In the Tendaho region, northwesterly and north-northeasterly trending faults predominate (UNDP, 1973).

North-northeasterly trending faults may have played only a minor role in the evolution of the Tendaho graben, where the dominant structural elements are northwest trending (UNDP, 1973). However, the intersection of these two fault trends appears to be a controlling factor governing the locations of current hydrothermal activity (UNDP, 1973). Inside the Tendaho Rift, lacustrine and alluvial plains alternate with zones where basalts crop out as northwest-oriented elongated fault blocks. Evidence for active northwest-striking faults includes aligned steaming grounds, fumaroles and hydrothermal deposits in the sediments within the Dubti plantation (Aquater, 1995).

According to the stratigraphy under the graben floor (revealed by geophysics and drilling), the rock units are grouped into:

- Upper unit - thick sedimentary sequence consisting of fine- to medium-grained sandstone, siltstone and clay, probably intercalated by basaltic lava sheets; and
- Lower unit - basaltic lava flows of the Afar stratoid series.

The geology of the Dubti-Semera area was mapped at a scale of 1:50,000 and the following units were identified (Megersa and Getaneh, 2006) (Figure 12). The rift margin complex of the study area, represented by stratified rift margin basalt, and the rift axis complex comprised of volcanic and sedimentary sequences.

The rift axis volcanic group of the study area, found in the axial range of Tendaho rift, includes: Ayrobera-Semera water-laid pyroclastic and sedimentary sequence, Semera basalt, Kurub basalt, Geblaytu rhyolitic rocks, Geblaytu scoria and Geblaytu-Asboda fresh pahoehoe basalt and hyaloclastite. Sedimentation of fluvial, lacustrine and eoline have been simultaneously carried with the axial volcanic activity, mainly in the graben area. Eolian deposit is the dominant surface sedimentary unit at present. The measured surface temperatures in geothermal manifestations mainly fall in the range 65-100.3ºC (Megersa and Getaneh, 2006).

In Tendaho geothermal field, six wells were drilled from 1993 to 1998. Wells TD1, TD2 and TD3 are deep wells with depths of 1550, 1881 and 1989 m, respectively. Wells TD4, TD5, and TD6 are shallow wells with depths of 466, 516 and 505 m, respectively. Wells TD2, TD4, TD5 and TD6 are productive.

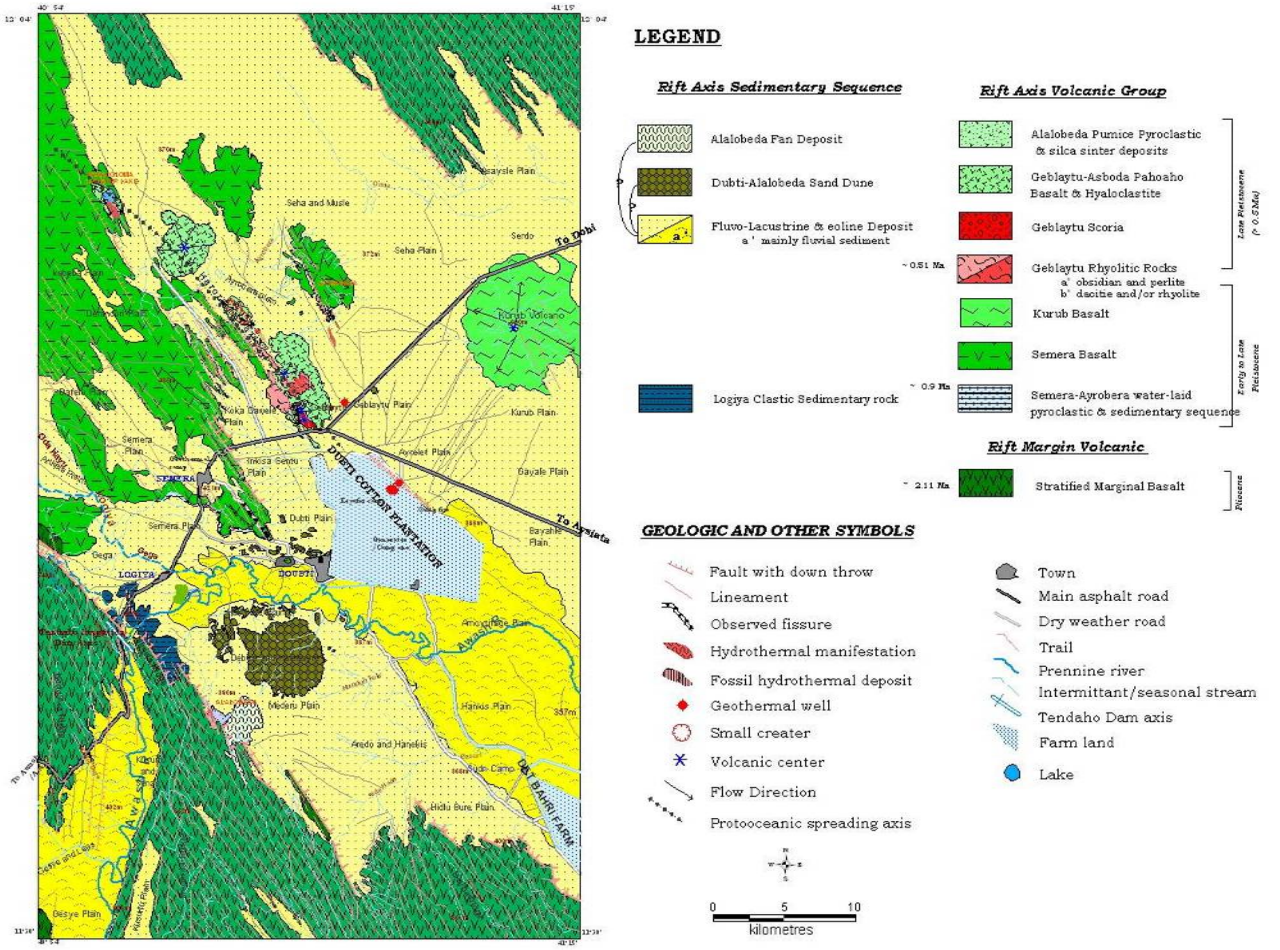

FIGURE 12: Geological map of Tendaho graben (Megersa and Getaneh, 2006)

4.2.2 Previous geophysical work

Regional and semi-detailed geophysical studies have been carried out in the Afar Depression and Tendaho geothermal field, with the aim of investigating the deep structures and to delineate a possible geothermal reservoir. The methods include magneto-telluric (MT) (e.g. Berktold, 1975); vertical electrical sounding (VES), magnetics and gravity survey (e.g. Aquater, 1980) among others.

In 1971 a MT survey was carried out in the Afar region to investigate the deep electrical resistivity distribution (Berktold, 1975). The survey included measurement of the electric field in 36 temporary stations along three profiles for a total length of 900 km. Profile I of the MT survey which trends east-west (Dessie-Bati-Serdo), intersects the study area. Results indicate that in the Afar Depression and the marginal parts of the western plateau, the resistivity is decreasing from 200 to 500 ohm-m in the uppermost kilometres to 10-50 ohm-m at a depth of about 15 km (Berktold, 1975). The anomalously low resistivity beneath Afar and marginal parts of the western plateau was interpreted as an anomalously high temperature of 800-1000˚C at a depth of about 15 km and a temperature gradient of about 60˚C/km (Berktold, 1975).

In 1972 five deep seismic refraction profiles 120-250 km long were run in the Afar lowland and on the western Ethiopian plateau (Berckhemer and Baier, 1975). In one profile, the crustal thickness was estimated to be beween 22 and 25 km with a 7.7 km/s mantle velocity; whereas in another profile the estimated crustal thickness was about 24 km and mantle velocity 7.6 km/s. According to Berckhemer

and Baier (1975), the interpretation suggests a crustal thinning and upwelling of hot upper-mantle material beneath Afar.

A gravity survey (between Tendaho, Serdo and Asayita) was conducted by Searle and Gouin (1971) in an area of 1000 km². The authors produced a Bouguer anomaly map using an average crustal density of 2.67 Mg/m³. The main feature of the map is a decrease in Bouguer gravity from -40 mGal to the north to -55 mGal along the Awash River in the south, mainly caused by the accumulation of sediments in the Awash Basin. A few localized Bouguer gravity anomalies were observed along the southern edge of the surveyed area. A relatively high Bouguer gravity is located near Tendaho village and a low near Dubti plantation.

An aeromagnetic map produced by Aquater (1979) showed a complex pattern of short positive and negative lineations. These were interpreted by Aquater (1979) as being related to a short spreading segment that has been active in the last four million years. One of these anomalies is located in the survey area along the Manda-Hararo volcanic range.

In 1971, the Hunting Geology and Geophysics Ltd. conducted an airborne infrared survey of the geothermal prospects in Ethiopia including the Tendaho area. The infrared survey was able to detect hot grounds in Tendaho that were not recognized by previous ground surveys.

Vertical electrical sounding (VES) data was acquired by Aquater (1980). In this survey, the depth of the investigation reached a maximum of one km and the data lacked resolution in differentiating layers within the sedimentary and basaltic sequences. In addition, Aquater (1980) occupied 2086 gravity stations in the Tendaho area. The NW-SE trending gravity low near Tendaho plantation is related to a depression of the high-density substratum. A strong positive Bouguer gravity anomaly centred over the Ayrobera area may be due to a dense intrusive body in the fluvial-lacustrine sediment system (Aquater, 1980). Aquater (1980) has also produced a total field magnetic map that shows a general NW-SE magnetic anomaly. The anomaly extends from northwest to southeast following the Tendaho graben axis with minor anomaly interruptions attributed to near-surface inhomogeneities.

Aquater (1980, 1996) drilled nine temperature gradient wells to map the subsurface temperature distribution in the Tendaho graben and Logiya areas. But, due to the shallow depths of the boreholes (76.6-173.5 m), the reservoir temperature is masked by the thick sedimentary layers and the presence of hot or cold shallow aquifers. The micro seismic survey (Aquater, 1995) in the Tendaho graben has indicated that the hypocenters of the seismic events are distributed in a NW-SE direction and to a depth between 5 and 10 km.

A geophysical survey by Oluma et al. (1996) consisted of Schlumberger traversing, head-on resistivity profiling, and vertical electrical sounding (VES) at three well sites (TD1, TD2 and TD4). Sixty line km gravity surveys were also conducted centring on the active thermal manifestations of the Tendaho graben. The result of AB/2=500 m resistivity map indicated a prominent anomaly with its roots in the southeast part**.** The result of the resistivity map for AB/2=1000 m showed a narrow northeast elongation of a low-resistivity zone. The dominant regional trends, i.e., northwest and northeast, are the major structures controlling the flow of hot geothermal fluids.

A gravity survey by Lemma and Hailu (2006) indicated a broad high Bouguer anomaly in Ayerobera area and a low Bouguer anomaly in the Dubti plantation area. These contrasting Bouguer anomalies may indicate the presence of a ENE-WSW trending regional crustal discontinuity (a fault). The high Bouguer and low total magnetic field anomalies at Ayrobera and Gebelaytu plains may indicate the presence of an intrusive body or might be associated with deposition of hydrothermal minerals on the volcanic rocks. The geothermal manifestations at Dubti plantation and Ayrobera areas lie in a NW-SE trending fault system as seen on magnetic and gravity anomaly maps (Lemma and Hailu, 2006).

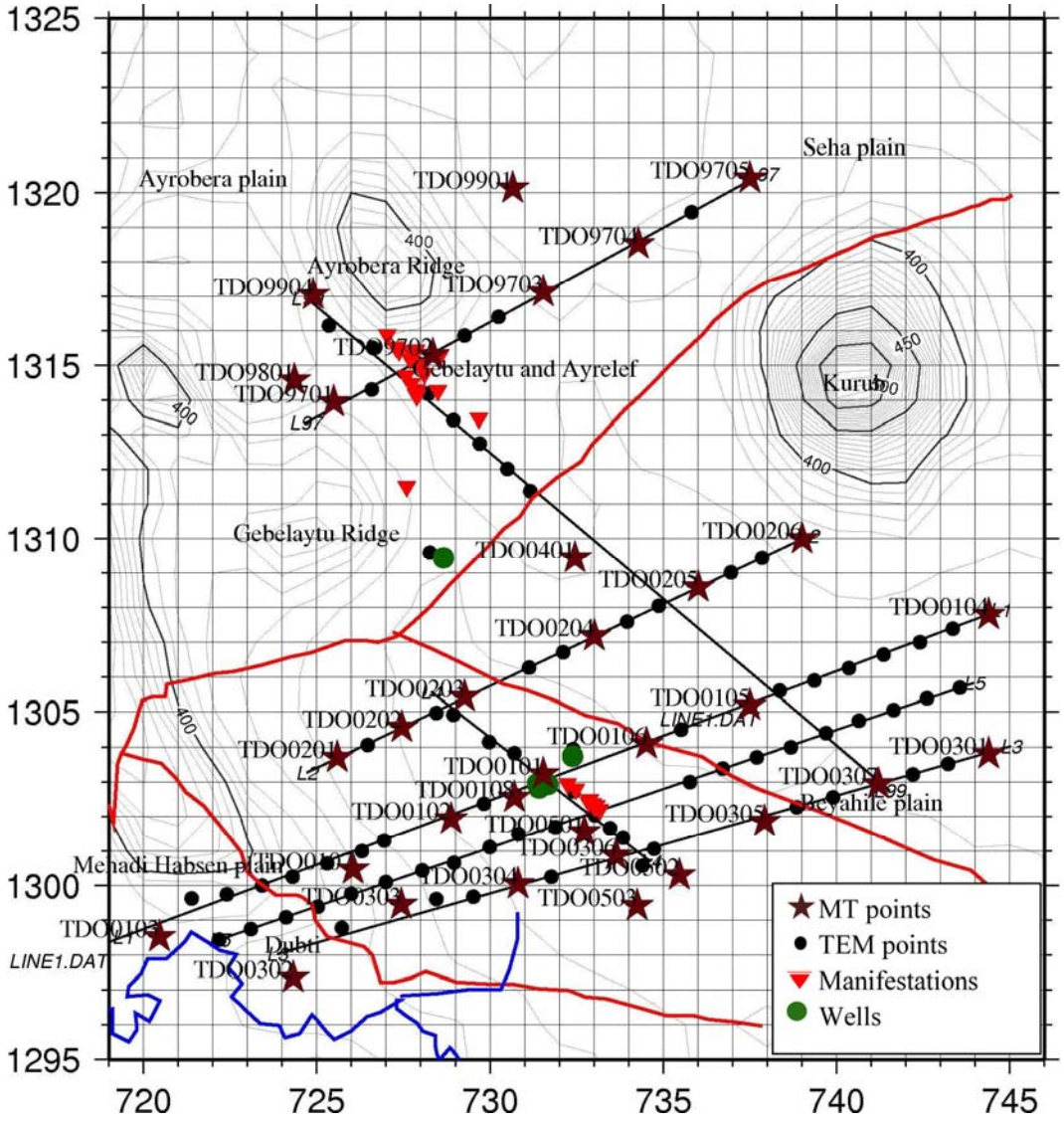

FIGURE 13: Location of MT and TEM soundings (UTM 37, datum: ADINDAN-Ethiopia, in km)

4.3 TEM and MT surveys

MT and TEM surveys were conducted as part of the "Tendaho shallow geothermal resource evaluation project" which started in 2005. This work was done by joint collaboration of experts from BGR (German Geological Survey) and Ethiopian Geological Survey from January 23 to February 23, 2007. A total of 102 TEM soundings were conducted using a central-loop TEM in the Tendaho geothermal field. About 21 soundings were done in Ayrobera area, while the remaining soundings were carried out at Dubti plantation and in the Kurub area (Figure 13). The TEM instruments used for the survey were from Geonics, and consist of the following (Geonics, 1999):

- Transmitters - TEM 47 and TEM 57 (maximum loop current of 20 A);
- PROTEM digital receiver;
- Receiver coils (31.4 m² and 100 m² effective area);
- Honda motor generator - 120/240 VAC/60Hz/500W.

In almost all the soundings, a 100 m × 100 m transmitter wire loop was used. A reference cable was used to link the transmitter and the receiver. A half duty square wave current was transmitted at

frequencies of 237.5, 62.5, 25, 6.25, 2.5, 0.625 and 0.25 Hz. The data from the PROTEM Digital Receiver was transferred to a personal computer for processing.

A total of 51 MT soundings were conducted in Tendaho geothermal field, while 26 soundings were used as remote reference soundings at Ayrobera and Gebelaytu plain. The remaining soundings were taken along profiles crossing Dubti plantation and the Kurub area. The distance between the MT stations varies between 3 and 5 km (Figure 13).

The instruments used for MT measurement were a pair of Metronix units. The system consists of the following units:

- ADU-06 (analog digital unit data logger) with 5 channels;
- Induction coil magnetometers MFS-06;
- Porous pot type electrodes of dipole length 100 m;
- Batteries 12 V / 80 Ah;
- Cables.

The control of the ADU was maintained using the control software GMS207b which is run under Windows operating system. Data was stored on the built–in flash disk on the ADU. The electric and magnetic field sensors were connected directly to the ADU-06. The induction coil covered a wide frequency range from 0.00025 Hz up to 10 kHz.

4.4 Data processing and interpretation of the TEM and MT

TEMX program was used to read TEM raw data files acquired from the PROTEM digital receiver of Geonics. The program calculates averages and standard deviations of repeated transient voltage measurements and calculates late time apparent resistivity as a function of time. The program has a graphical interface and offers a possibility of editing raw data by rejecting some of the noisy readings.

The program TEMTD was used to perform joint 1D inversion of MT and TEM data for the determination of the impedance tensor which is rotationally invariant. It can also be used to invert only TEM or MT data. In the case of joint inversion, it determines the static shift parameter for the MT data. The program assumes horizontally layered earth models of TEM and MT data during 1D inversion. For TEM data, the program assumes that the source loop is a square loop and that the receiver coil is at the centre of the source loop. The current wave form is assumed to be half-duty bipolar semi-square wave with exponential current turn-on and linear current turn-off. The program is written in ANSI-C and runs under UNIX/LINUX operating systems. The program was written by Knútur Árnason of ISOR (Árnason, 2006). It uses the Gnuplot graphics program for graphical display during the inversion process. The inversion algorithm used in the program is the Levenberg-Marquardt non-linear least square inversion as described by Árnason (1989). The misfit function is the root mean square difference between measured and calculated values (Árnason, 1989). The program offers the possibility to keep models smooth with respect to resistivity variations between layers and layer thicknesses. The program can be used to perform Occam's inversion. The file input for TEMTD is *.inv file produced by the program TEMX for TEM. For MT data the program assumes standard EDI format. Appendix I shows examples of TEM soundings with 1D inversion, while Appendix II shows examples of 1D joint inversion of TEM and MT data. All soundings used and interpreted are presented with their 1D interpretation in a special appendix report, published separately (see Lemma, 2007).

GMS207b program was used to download time series data from ADU-06 to the computer. The time series data was then processed by the Mapros program supplied by Metronix (Friedrichs, 2005). MAPROS allows editing of the time series data. Fourier transformed data were obtained from it. A resultant file which was created in MAPROS was exported to electrical data interchange (EDI) format for inversion.

Signal strength was weakest in the so-called 'dead band' around 1Hz in the MT data. Data quality was poor in this frequency range. On the TEMTD program, an option was included to suppress MT data in those period (frequency) intervals. TEM data were collected at almost all sites to determine shallow resistivity structures. These can be used to help resolve static shift arising from near surface distortions.

The programs TEMRESD, TEMMAP and TEMCROSS were used in plotting both MT and TEM data. The programs run under UNIX/Linux environment and the code was written by H. Eysteinsson of ISOR - Iceland Geosurvey (Eysteinsson, 2007). TEMRESD is used to plot iso-resistivity maps for Occam inverted models at any depth. TEMMAP is used to plot the location of TEM and MT soundings on a map in UTM coordinate system. TEMCROSS is used to plot resistivity cross-sections for 1D layered earth models. All three programs use the GMT (Generic Mapping Tools) program package.

5. RESULTS OF THE TEM AND MT SURVEYS

The results of the TEM and MT surveys are presented as resistivity cross-sections and iso-resistivity maps.

5.1 TEM cross-sections

Resistivity cross-section L1, Figure 14, runs from Dubti area in the southwest, passes close to well TD4 at the centre and ends southeast of Kurub volcano. The cross-section is characterized by a low-resistivity anomaly of <10 Ωm at 200 m depth from the surface. This low resistivity is associated with the sedimentary formation in the area.

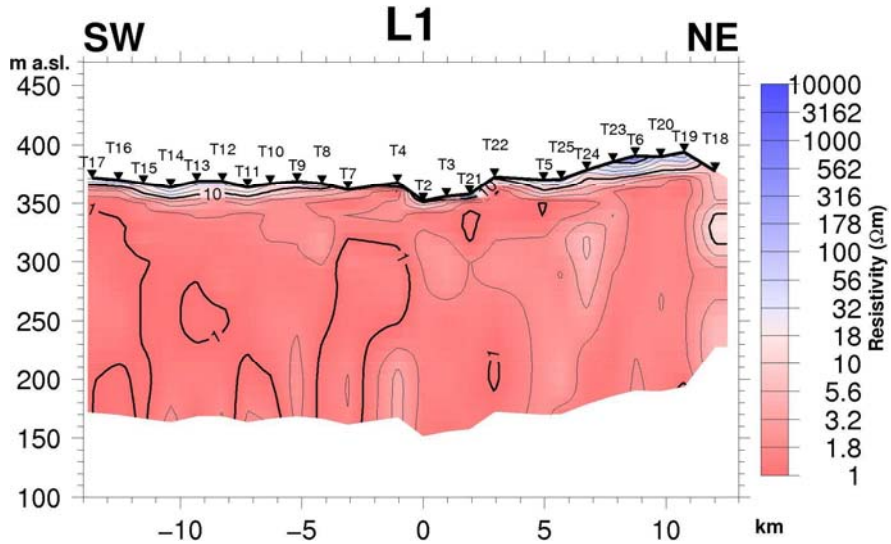

FIGURE 14: TEM resistivity cross-section L1

Resistivity cross-section L2, Figure 15, runs from Mehadi Habsen plain in the southwest to Kurub in the northeast. The cross-section is characterized by a low resistivity of <10 Ωm for the whole depth of investigation. This low resistivity can be correlated to thick sediments in the area.

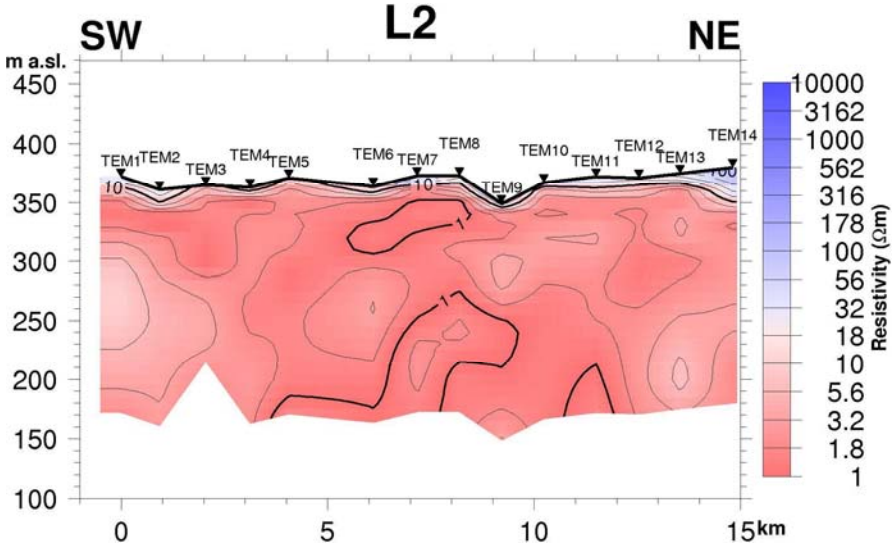

FIGURE 15: TEM resistivity cross-section L2

Resistivity cross-section L3, Figure 16, which runs from Dubti in southwest to Behyahile plain in the northeast, is also characterized by low resistivity of <10 Ωm for the total depth of 200 m. This low resistivity can be correlated to the sedimentary formation in the area.

Resistivity cross-section L4, Figure 17, runs across the profiles L1, L2, L3, and L5 from northwest to southeast. The cross-section is characterized by a low-resistivity anomaly ≤10 Ωm for the whole depth of 200 m.

Resistivity cross-section L5, Figure 18, which runs southeast across part of Tendaho plantation to Behyahile plain in northeast is also characterized by low resistivity of <10 Ωm for the total depth of 200m.

Resistivity cross-section L97, Figure 19, runs from Gebelaytu ridge in the southwest to Seha plain in the northeast. In the southwest portion of the cross-section, high resistivity >100 Ωm underlies low resistivity under TEM9701. In the northeast part of the cross-section, the top 80 m are characterized by a resistivity <3.2 Ωm. The high resistivity on the southwest close to Gebelaytu ridge is

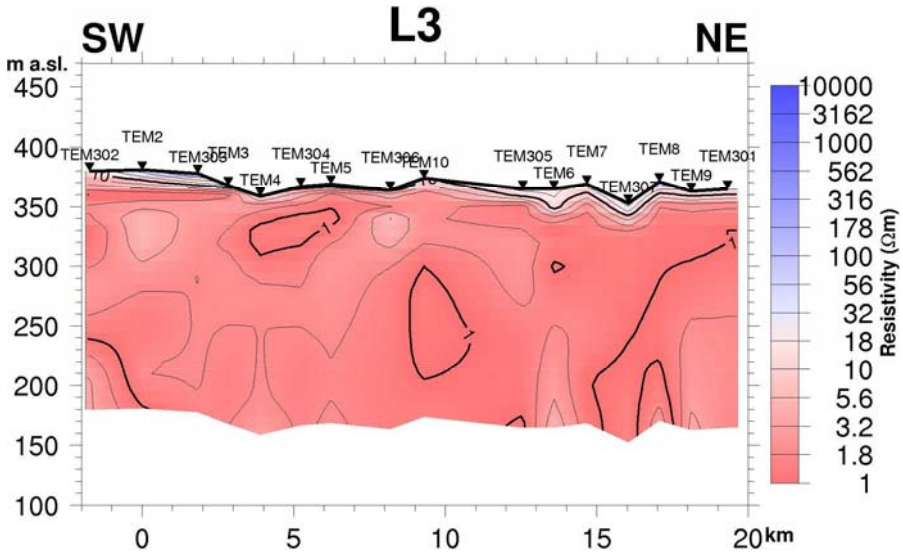

FIGURE 16: TEM resistivity cross-section L3

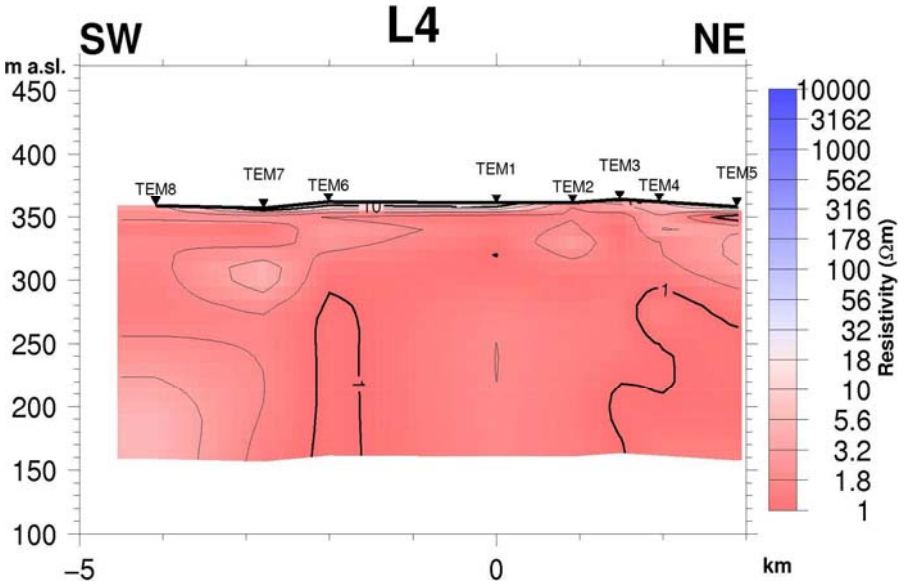

FIGURE 17: TEM resistivity cross-section L4

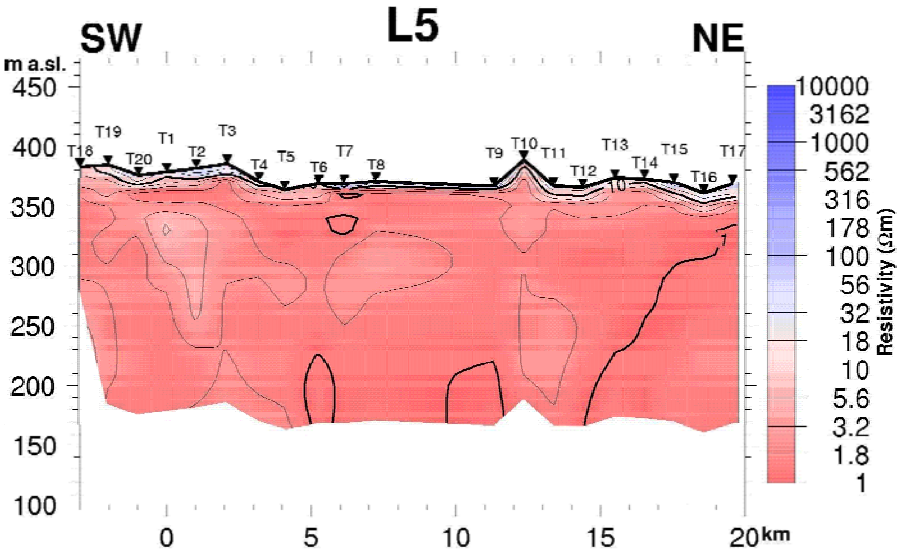

FIGURE 18: TEM resistivity cross-section L5

associated with upper extrusive basalts. A relatively high resistivity of >10 Ωm is observed in the bottom part of the cross- section. This is correlated to basalts intercalated in the sediment.

Resistivity cross-section L99, Figure 20, runs from Beyahile plain in the southeast to Ayrobera plain in the NW. The resistivity cross-section in the southeast part of the profile is characterized by resistivity < 3.2 Ωm. The northwest part of the profile has resistivity values >10 Ωm. In general, the resistivity is increasing from south-east to northwest along the profile.

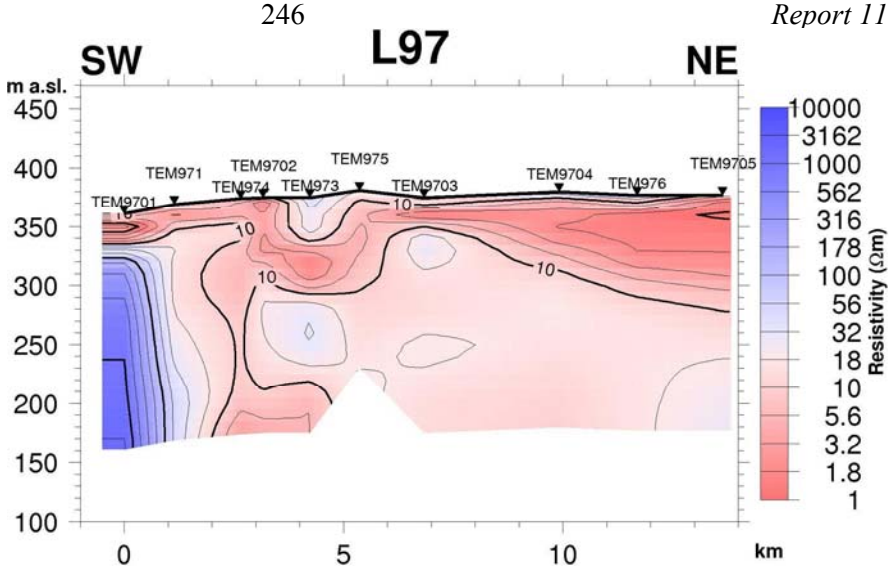

FIGURE 19: TEM resistivity cross-section L97

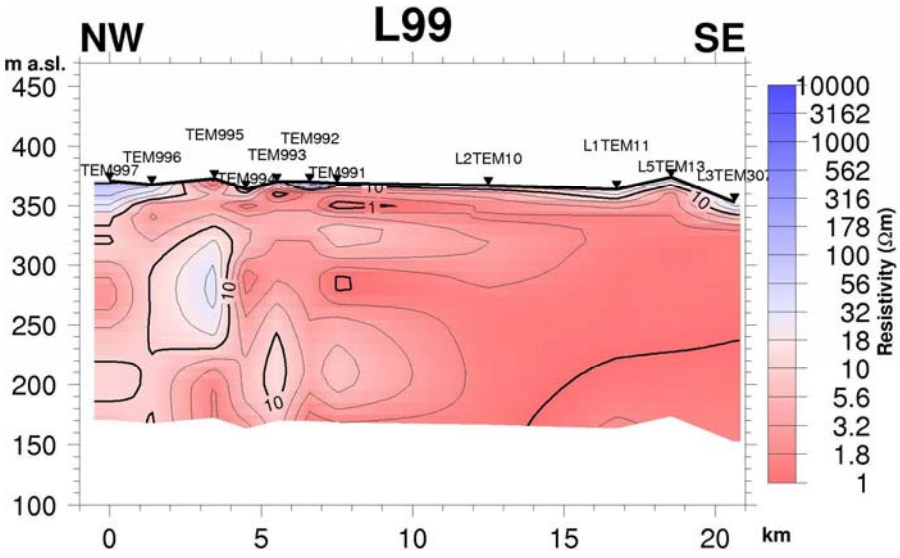

FIGURE 20: TEM resistivity cross-section L99

5.2 TEM resistivity maps

Iso-resistivity map at 300 m a.s.l, showing resistivity at an average depth of 60 m from the surface is given in (Figure 21). At the Dubti plantation, Beyahile plain and south of Kurub volcanic complex the map shows resistivity below 3.2 Ωm. In the northwest sector of the map, Gebelaytu plain is characterized by resistivity of > 10 Ωm. In this sector, high resistivity of more than 100 Ωm is observed near Gebelaytu ridge. This high resistivity can be correlated to upper extrusive basalts found in the area. In general, at this depth the resistivity is increasing from southeast to northwest.

Iso-resistivity map at 200 m a.s.l. is seen in Figure 22, showing resistivity at an average depth of 160 m from the surface. It is similar to the map in Figure 21, except for the high resistivity near Gebelaytu ridge, > 300 Ωm.

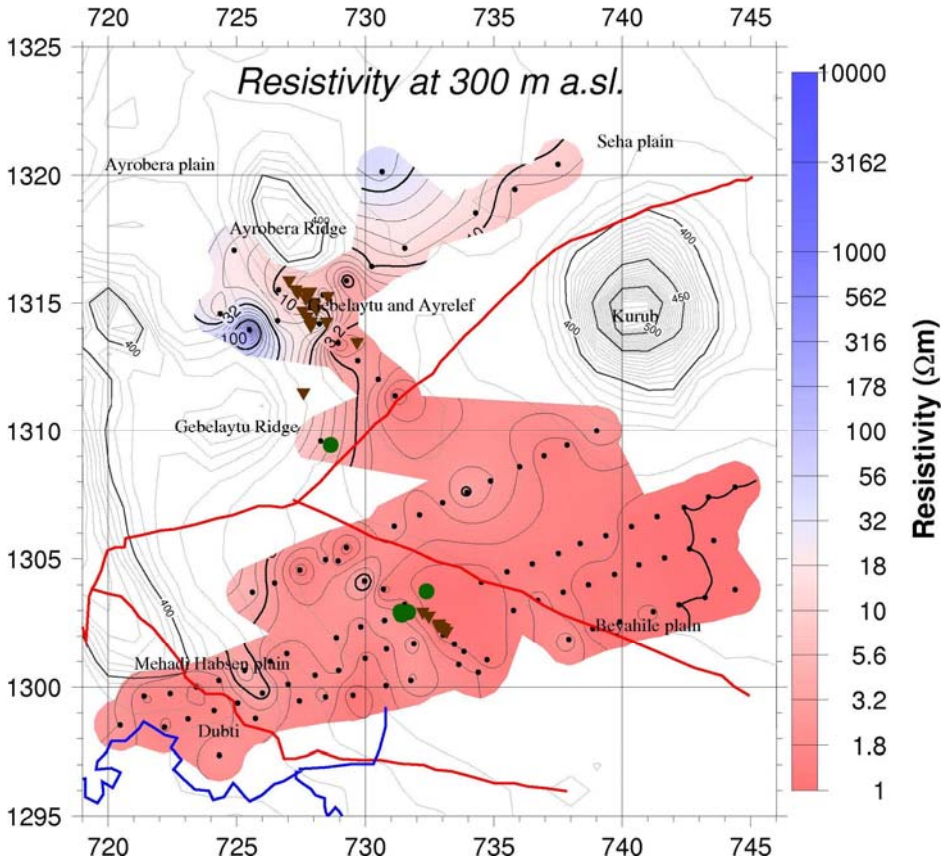

FIGURE 21: TEM resistivity map at 300 m a.s.l.

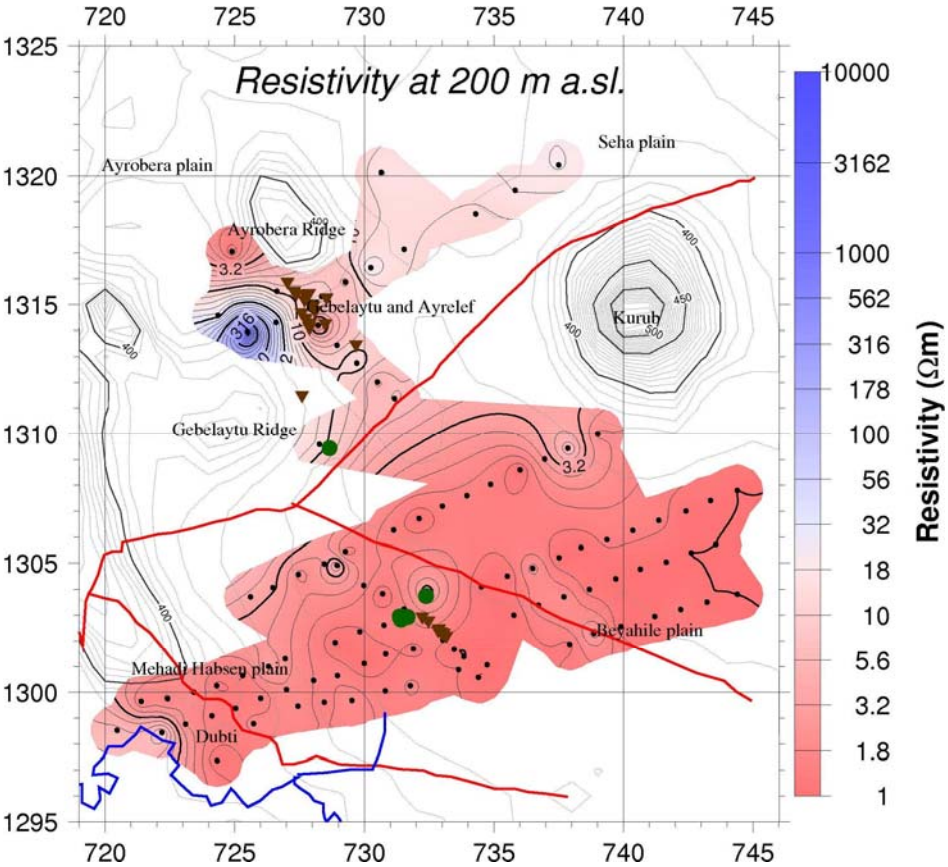

FIGURE 22: TEM resistivity map at 200 m a.s.l.

5.3 MT cross-sections

MT cross-section, L1, Figure 23, runs from Dubti in the southwest, passes the geothermal manifestations near the shallow well TD4 and ends southeast of Kurub volcano. A low resistivity of about 1 Ωm is observed across the cross-section to a depth of 100 m a.s.l., associated with sediments. In the northeast part of the cross-section, a relatively high resistivity is observed from a depth of 0 to 200 m b.s.l. This correlates to basalts intercalated in sediments. Another low-resistivity layer of 1 Ωm is observed from 200 to 500 m b.s.l. This is associated with sediments or lateral flow of geothermal fluid or a fracture zone. A high-resistivity anomaly of >100 Ωm is observed under TDO0106 from a depth of 1000-2000 m b.s.l. A similar anomaly is observed under TDO0103 and TDO0107 from 1200 to 2000 m b.s.l. This high resistivity can be associated to the less permeable Afar stratoid basalts. Between these two high-resistivity structures, there is a low-resistivity zone under soundings TDO0107 and TDO0108 at the bottom part of the cross-section. This could be due to the presence of a fracture zone in the basalts which may give rise to higher permeability and higher temperature and may indicate upflow of geothermal fluid into the system.

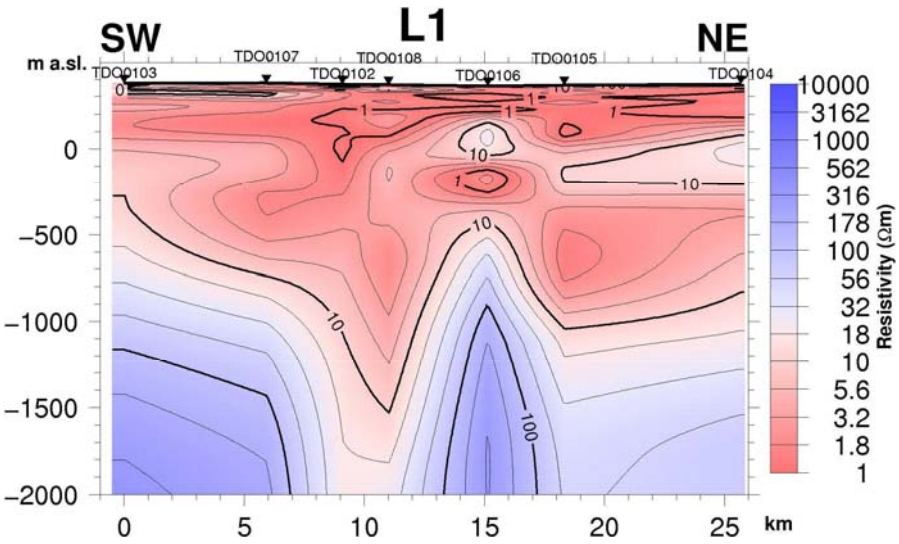

FIGURE 23: MT resistivity cross-section L1

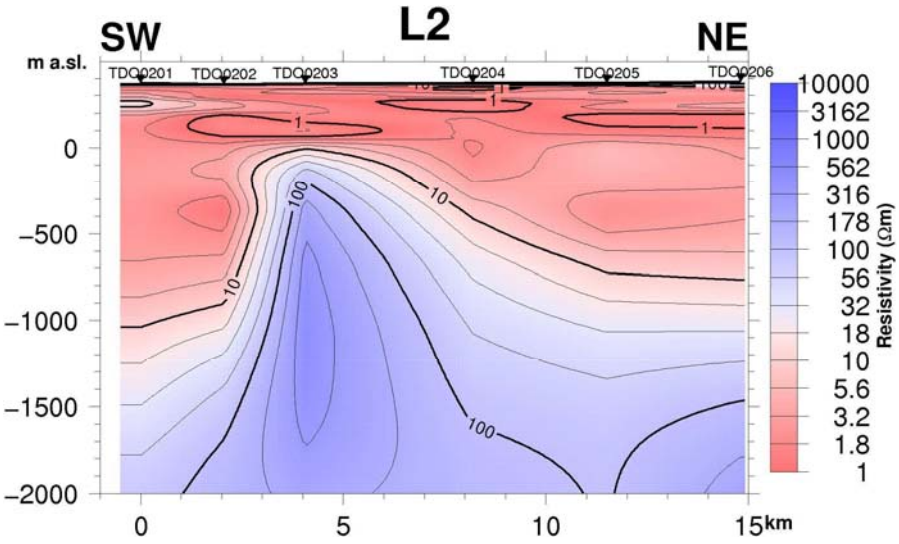

FIGURE 24: MT resistivity cross-section L2

MT cross-section L2, Figure 24, runs from Mehadi Habsen plain in the southwest to Kurub volcanic complex in the northeast. A low-resistivity layer, ≤ 10 Ωm, is observed along the whole cross-section to a depth of 0 m a.s.l. In the southwest section under soundings TDO0201 and TDO0202, this low resistivity extends to a depth of 1000 m b.s.l. The same resistivity structure extends to 800 m b.s.l. in the northeast part of the cross-section under soundings TDO0205 and TDO0206. This low-resistivity structure can be correlated to sediments. A broad high resistivity of ≥ 100 Ωm is observed along the cross-section at an average depth of 1000 m b.s.l. This high resistivity is updoming near the southwest sector of the section, especially under TDO0203. The high resistivity at the bottom part of the cross-section is associated with the Afar stratoid series basalts.

MT cross-section L3, Figure 25, runs from Dubti in the southwest to Behyahile plain in the northeast. A low resistivity ≤ 10 Ωm is observed to a depth of 0 m at sea level. A broad high resistivity of ≥ 100 Ωm is observed under the low resistivity to a depth of 2000 m b.s.l. The low resistivity can be associated with sediments and the high resistivity to the Afar stratoid basalts.

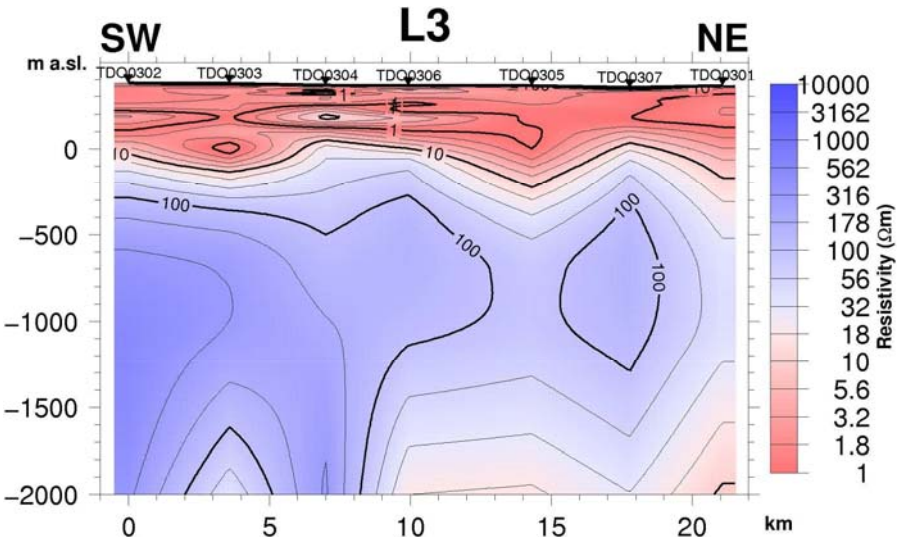

FIGURE 25: MT resistivity cross-section L3

MT cross-section L97, Figure 26, runs from Gebelaytu ridge in the southwest to Seha plain in the northeast. A high-resistivity anomaly ≥ 100 Ωm is observed at a shallow depth of about 200 m a.s.l in the southwest part of the cross-section under sounding TDO9712. A relatively high resistivity of ≥ 10 Ωm is observed on the northeast part of the cross-section at the same depth. This high resistivity can be correlated to basalts in the area. The rest of the cross-section is characterized by low resistivity, ≤ 10 Ωm to a depth of 300 m b.s.l. This low resistivity is associated with sedimentary formation or geothermal fluid circulation in the formation. A high-resistivity anomaly, >100 Ωm, is observed under TDO9712 from a depth of 400 m to 2000 m b.s.l. A similar anomaly is observed under TDO9742 and TDO9705 from 500 m to 2000 m b.s.l. This high resistivity is associated with less permeable Afar stratoid basalts. Between these two high-resistivity structures, there is a low-resistivity zone under soundings TDO9702 and TDO9703 in the Afar stratoid basalts. This anomaly is interpreted as a fracture zone in basalts where geothermal fluids circulate.

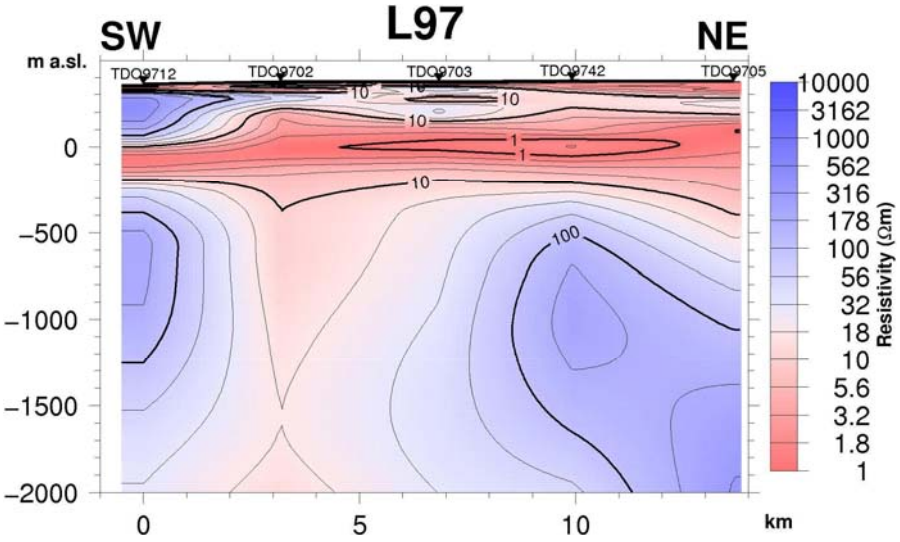

FIGURE 26: MT resistivity cross-section L97

7. CONCLUSIONS AND RECOMMENDATIONS

- The TEM method revealed low resistivity of < 3.2 Ωm at the shallow depth of about 200 m in the Dubti area compared to higher resistivities in the Ayrobera area.
- In MT cross-sections L1 and L97, the low resistivity at shallow depth can be correlated to sedimentary formations (clay, siltstone and sandstone), lateral flow of geothermal fluid, fracture zone or alteration mineralization. The high resistivity at depth below the low resistivity can be

associated to the less permeable Afar stratoid series basalts. A low-resistivity zone bounded between high resistivity in the basalts is interpreted as a fracture zone which gives rise to higher permeability and higher temperature and may indicate upflow of geothermal fluids. The fracture zone inferred from MT cross-sections coincides with the surface geothermal manifestations in the Dubti and Ayrobera areas.

- In MT cross-section L1, the low-resistivity zone between MT soundings TDO0107 and TDO0106 may represent a shallow sedimentary reservoir at a depth of 200 m b.s.l. and a deep basaltic reservoir at 1000 m b.s.l. which was also observed during well testing and reservoir engineering study results of Tendaho geothermal field (Amdeberhan and Björnsson, 2000).
- The fracture zones interpreted from MT cross-sections L1 and L97 correlate to the NW-SE trending structures inferred from the gravity and magnetic survey for the area (Lemma and Hailu, 2006, see Appendices III and IV). The fracture zone inferred from the MT cross-sections also coincides with the surface geothermal manifestations in the Dubti and Ayrobera areas.
- In MT cross-sections L2 and L3, a low resistivity is underlain by a high-resistivity formation. The low resistivity can be correlated to sedimentary formation, but the high resistivity can be associated to the Afar stratoid series basalts.

The TEM survey gave information to a depth of 200 m. In order to get deeper information with this method, it would be helpful to use a large square loop of 300 m × 300 m, a separate power module and a big generator. The fracture zones on MT cross-sections L1 and L97 are not well resolved because of large MT station spacing. Therefore, this study recommends that additional TEM (with large loop area) and a systematically gridded long period MT survey be carried out to delineate the size and boundary of the geothermal resource in the Tendaho geothermal field.

ACKNOWLEDGEMENTS

I would like to express my gratitude to the director of the UNU-GTP, Dr. Ingvar B. Fridleifsson, and the deputy director, Mr. Lúdvík S. Georgsson, for nominating me for this very special training and Ms. Þórhildur Ísberg for every arrangement made for coming to the training and for help during the course. I am greatly indebted to my supervisors, Mr. Knútur Árnason assisted by Dr. Hjálmar Eysteinsson and Mrs. Ragna Karlsdóttir of ISOR's geophysics department, for their guidance and sharing of knowledge and experience with me.

I wish to express my sincere gratitude to the Geological Survey of Ethiopia for the chance and support to participate in this training. Also I thank Dr. Meseret Teklemariam and the entire geothermal staff for their support during my preparation for the course. I wish to give my thanks to all lecturers and staff members at Orkustofnun and ISOR for their comprehensive presentations and willingness to share their knowledge and experience.

REFERENCES

Amdeberhan, Y., and Björnsson, G., 2000: Well testing and reservoir engineering studies at the Tendaho geothermal field. *Proceedings of the World Geothermal Congress 2000, Kyushu-Tohoku, Japan,* 901-907.

Aquater, 1979: *Geothermal resources exploration project Tendaho area - Prefeasibility study*. EIGS and Ministry of Foreign Affairs of Italy, San Lorenzo in Campo.

Aquater, 1980: *Geothermal resource exploration project Tendaho area, feasibility study - Phase II*. EIGS and Ministry of Foreign Affairs of Italy, San Lorenzo in Campo.

Aquater, 1995: *Micro seismic study*, *final report*. EIGS and Ministry of Foreign Affairs of Italy, San Lorenzo in Campo.

Aquater 1996: *Tendaho geothermal project, final report.* MME, EIGS - Government of Italy, Ministry of Foreign Affairs, San Lorenzo in Campo.

Archie, R.G., 1942: The electrical resistivity log as an aid in determining some reservoir characteristics. *Trans. AIME, 146,* 54-67.

Árnason, K., 1984: The effect of finite potential electrode separation on Schlumberger soundings. *54th Annual International SEG Meeting, Atlanta, Extended abstracts*, 129-132.

Árnason, K., 1989: *Central-loop transient electromagnetic sounding over a horizontally layered earth*. Orkustofnun, Reykjavík, report OS-89032/JHD-06, 129 pp.

Árnason, K., 2006: *TEMTD (program for 1D inversion of central-loop TEM and MT data)*. ISOR, Reykjavík, short manual, 16 pp.

Árnason, K., Karlsdóttir, R., Eysteinsson, H., Flóvenz, Ó.G., and Gudlaugsson, S.Th., 2000: The resistivity structure of high-temperature geothermal systems in Iceland. *Proceedings of the World Geothermal Congress 2000*, *Kyushu-Tohoku, Japan,* 923-928.

Berckhemer, H., and Baier, B, 1975: Deep seismic sounding in the Afar region and on the highland of Ethiopia. *Proceedings of the International Symposium on the Afar Region and Related Rift Problems. Schweizerbart, I, Stuttgart,* 89-107.

Berktold, A., 1975: Magnetotelluric measurements in the Afar area. Afar Depression of Ethiopia. *Proceedings of the International Symposium on the Afar Region and Related Rift Problems, Schweizerbart, I, Stuttgart*, 262-275.

Berktold, A., 1983: Electromagnetic studies in geothermal regions. *Geophysical Surveys, 6*, 173-200.

Colorado School of Mines, 1999: *Introduction to geophysics*. Colorado School of Mines, web page: www.mines.edu/fs_home/tboy/GP311/MODULES/RES/main.html.

Dakhnov, V.N., 1962: *Geophysical well logging*. Q.Colo.Sch. Mines, 57, no. 2,445 pp.

Dobrin, M.B., and Savit, C.H., 1988: *Introduction to geophysical prospecting.* McGraw-Hill publ., NY, 867 pp.

Eysteinsson, H., 1998: *TEMRESD, TEMMAP and TEMCROSS plotting programs*. ÍSOR- Iceland GeoSurvey, unpublished programs and manual.

Flóvenz, Ó.G., Georgsson, L.S., and Árnason, K., 1985: Resistivity structure of the upper crust in Iceland, *J. Geophys. Res., 90-B12,* 10,136-10,150.

Friedrichs, B., 2005: *MAPROS (version 0.876b freeware), manual*. Metronix, 123 pp.

Geonics, 1999: *Operating Manual for PROTEM 67 D*. Geonics Ltd, Ontario, 58 pp.

Hersir, G.P., and Björnsson, A., 1991: *Geophysical exploration for geothermal resources. Principles and applications*. UNU-GTP, Iceland, report 15, 94 pp.

Kearey, P., and Brooks, M., 1994: *An introduction to geophysical exploration* (2nd edition). Blackwell Scientific Publ., London, 236 pp.

Keller, G.V., and Frischknecht, F.C., 1966: *Electrical methods in geophysical prospecting*. Pergamon Press, 527 pp.

Lemma, Y., 2007: *Appendices to the report "Magnetotelluric and transient electromagnetic methods in geothermal exploration, with an example from Tendaho geothermal field, Ethiopia"*. UNU-GTP, Iceland, report 11, appendices, 40 pp.

Lemma, Y., and Hailu, A., 2006: *Gravity and magnetics survey at the Tendaho geothermal field*. GSE, Addis Ababa, unpublished internal report, 23 pp.

Manzella, A., 2007: *Geophysical methods in geothermal exploration*. Italian National Research Council, International Institute for Geothermal Research, Pisa. Web page: http://cabierta.uchile.cl/revista/12/articulos/pdf/A_Manzella.pdf, 40 pp.

McNeill, 1994: *Principle and application of time domain electromagnetic techniques for resistivity sounding*. Geonics Ltd., Ontario, technical note TN 27, 15 pp.

Megersa, G., and Getaneh, E., 2006: *Geological, surface hydrothermal alteration and geothermal mapping of Dubti-Semera area, Tendaho geothermal field.* GSE, Addis Ababa, unpubl. report, 66 pp.

Oluma, B., Ayana, D., and Demisse, Y., 1996: *Geophysical survey of Tendaho geothermal field*. MME, EIGS, geothermal exploration project, unpubl. report, 23 pp.

Oskooi, B., Pedersen, L.B, Smirnov, M., Árnason, K., Eysteinsson, H., Manzella, A., and the DGP Working Group, 2004: The deep geothermal structure of the Mid-Atlantic Ridge deduced from MT data in SW Iceland. *Science Direct, 150, 183-195*.

Pellerin, L., and Hohmann, G.W., 1990: Transient electromagnetic inversion: A remedy for magnetotelluric static shifts. *Geophysics, 55-9,* 1242-1250.

Quist, A.S., and Marshall, W.L., 1968: Electrical conductances of aqueous sodium chloride solutions from 0 to 800°C and at pressures to 4000 bars. *J. Phys. Chem., 72,* 684-703.

Searle, R.C., and Gouin, P., 1971: *Gravity survey of the Tendaho-Asayita-Sardo region, Wollo, Ethiopia*. Geophysical Observatory of Addis Ababa University, Addis Ababa, technical report.

Simpson, F., and Bahr, K., 2005: *Practical magnetotellurics*. Cambridge University Press, Cambridge, UK, 254 pp.

Sternberg, B.K., Washburne, J.C., and Pellerin, L., 1988: Correction for static shift in magnetotellurics using transient electromagnetic soundings. *Geophysics, 53,* 1459-1468.

Ward, S.H, and Wannamaker, P.E., 1983: *The MT/AMT electromagnetic method in geothermal exploration*. UNU-GTP, Iceland, report 5, 107 pp.

UNDP, 1973: *Geology, geochemistry and hydrology of hot springs of the East African rift system within Ethiopia.* UNDP, NY, technical report DD/SF/ON/11.

Zhdanov, M.S., and Keller, G.V., 1994: *The geoelectric methods in geophysical exploration.* Elsevier, Amsterdam, 873 pp.

APPENDIX I: Examples of 1-D modelling of TEM using TEMTD

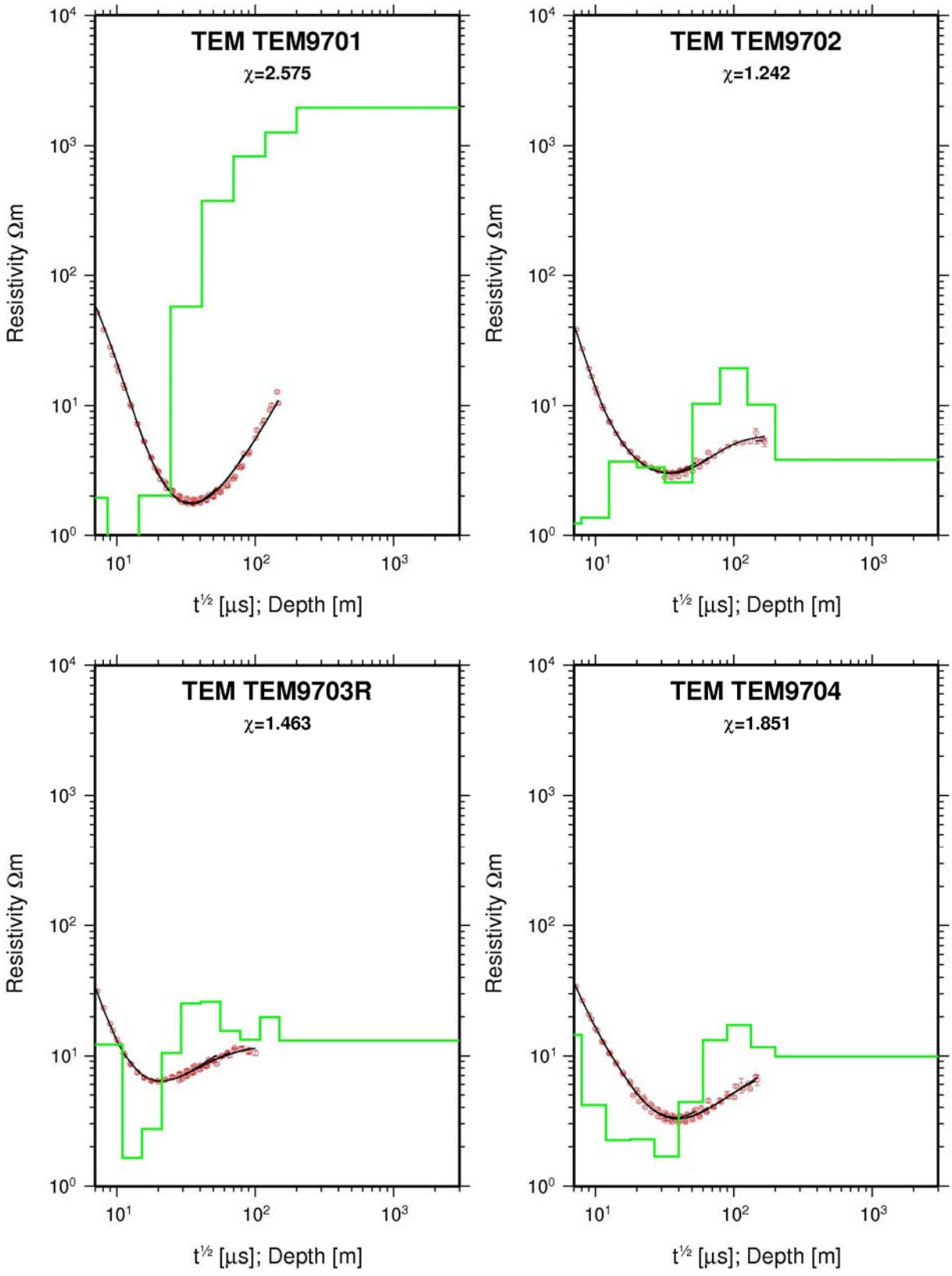

APPENDIX II: Examples of 1-D joint inversion of TEM and MT using TEMTD

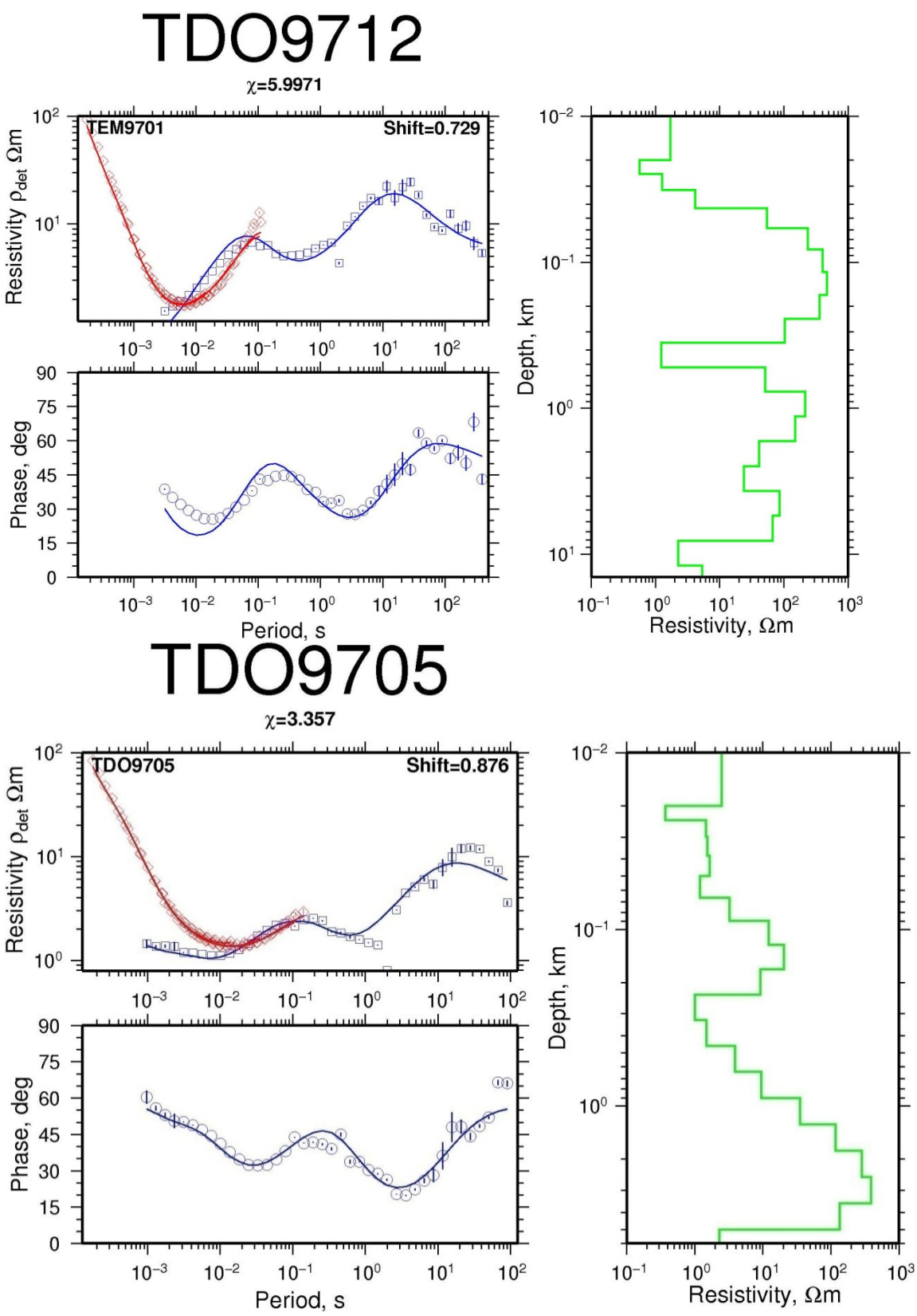

APPENDIX III: Residual gravity map of Tendaho geothermal field
(Lemma and Hailu, 2006)

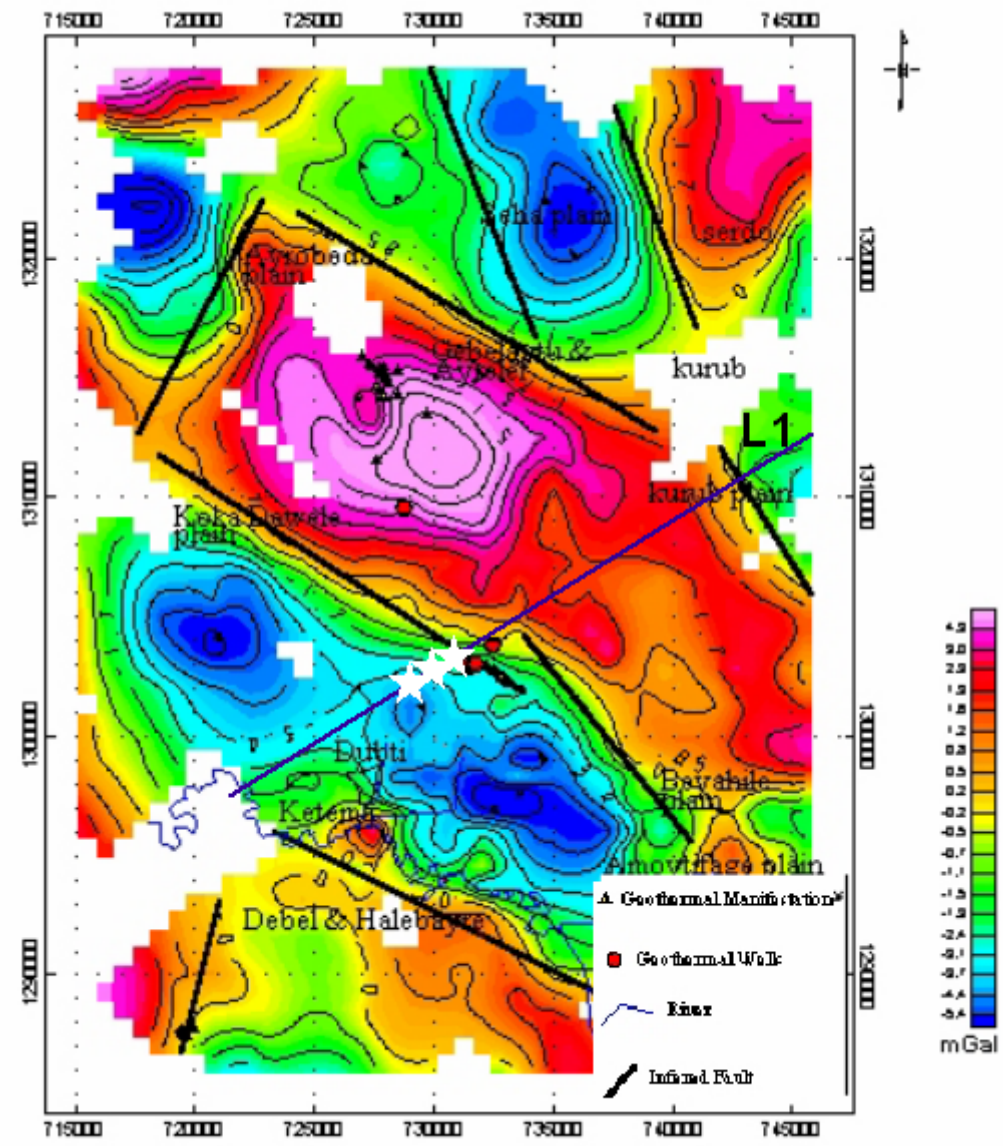

Legend: Thick black lines NW-SE direction = inferred faults (fractures);
Thin blue line L1 (SW-NE direction) = MT profile;
White star symbols = MT points crossed by NW-SE structure.

APPENDIX IV: Total field magnetic map of Tendaho geothermal field
(Lemma and Hailu, 2006)

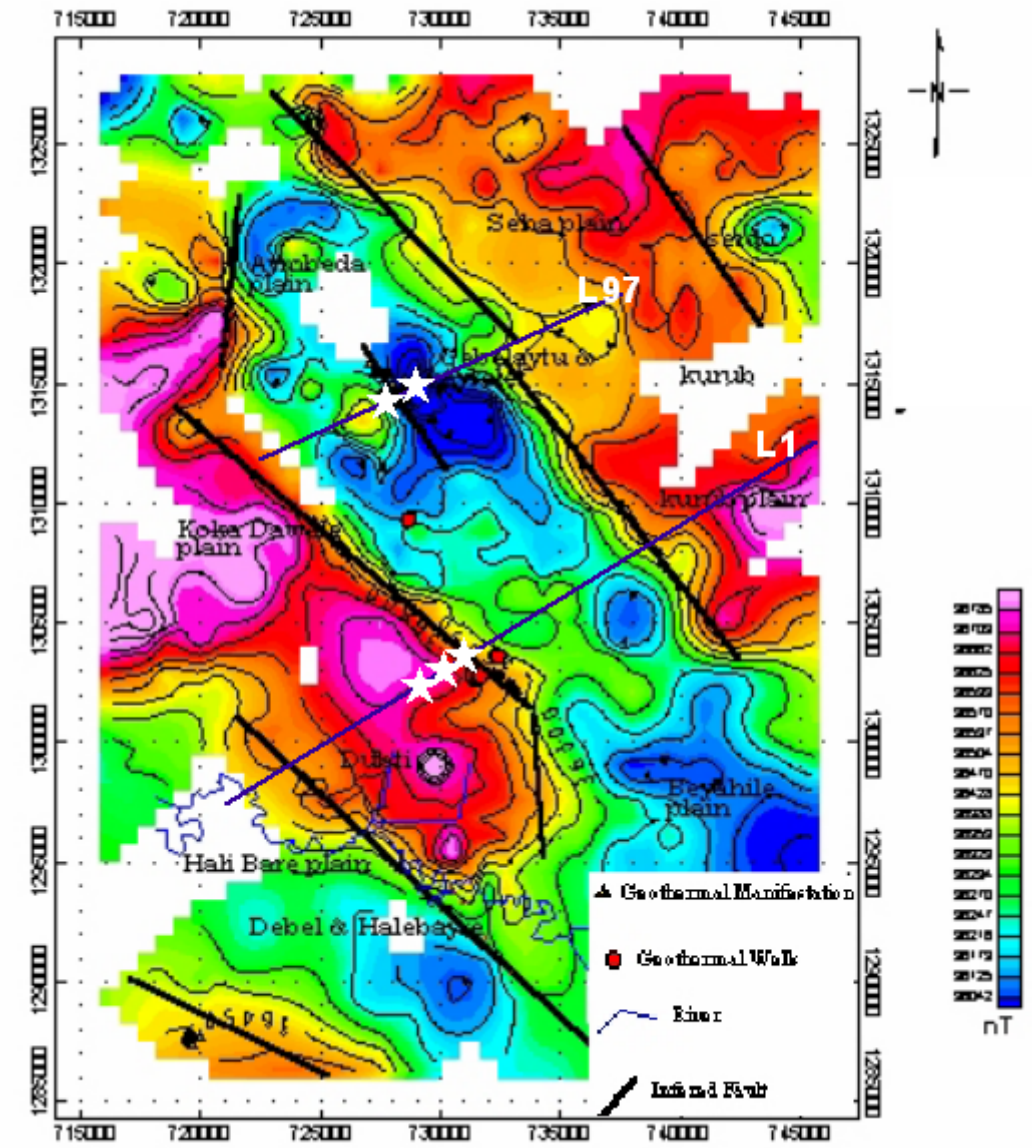

Legend: Thick black lines NW-SE direction show inferred faults (fractures);
Thin blue lines L1 and L97 (SW-NE direction) show MT profile lines;
White star symbols show MT points crossed by NW-SE structures.